Netherlands Journal of Sea Research
33 (3/4): 271-299 (1995)

SIMULATIONS OF THE NORTH SEA CIRCULATION, ITS VARIABILITY, AND ITS IMPLEMENTATION AS HYDRODYNAMICAL FORCING IN ERSEM

HERMANN J. LENHART, GÜNTHER RADACH, JAN O. BACKHAUS and THOMAS POHLMANN

Institut für Meereskunde der Universität Hamburg, Troplowitzstraße 7, D-22529 Hamburg, Germany

ABSTRACT

The rationale is given of how the gross physical features of the circulation and the stratification of the North Sea have been aggregated for inclusion in the ecosystem box model ERSEM. As the ecosystem dynamics are to a large extent determined by small-scale physical events, the ecosystem model is forced with the circulation of a specific year rather than using the long-term mean circulation field. Especially the vertical exchange processes have been explicitly included, because the primary production strongly depends on them. Simulations with a general circulation model (GCM), forced by three-hourly meteorological fields, have been utilized to derive daily horizontal transport values driving ERSEM on boxes of sizes of a few 100 km. The daily vertical transports across a fixed 30-m interface provide the necessary short-term event character of the vertical exchange.

For the years 1988 and 1989 the properties of the hydrodynamic flow fields are presented in terms of trajectories of the flow, thermocline depths, of water budgets, flushing times and diffusion rates. The results of the standard simulation with ERSEM show that the daily variability of the circulation, being smoothed by the box integration procedure, is transferred to the chemical and biological state variables to a very limited degree only.

1. INTRODUCTION

The ecological dynamics in the North Sea cannot be understood without the knowledge of its hydrographic and hydrodynamic state (Otto *et al.*, 1990; Fransz *et al.*, 1991). In setting up an ecosystem model for the North Sea the question has to be answered how much physical detail should be incorporated in the model. The characteristics of physical and biological dynamics have to be identified to give the answer. Therefore the scales of the governing physical processes are briefly reviewed and the circulation, salinity and current patterns (Otto *et al.*, 1990; Becker, 1990; Backhaus, 1990; Hainbucher *et al.*, 1986) are summarized before dealing with the implementation of transport into ERSEM for transporting nutrients and biota.

ERSEM is an ecosystem model which simulates the ecosystem dynamics in the various regions of the North Sea (Baretta *et al.*, 1995). These regions are not independent of each other but are connected by transport mechanisms. Advective and diffusive transports of water, abiotic and biotic substances generally play an important role in shelf seas such as the North Sea. Thus for a simulation of the North Sea ecosystem dynamics the physical transports cannot be neglected (Baretta *et al.*, 1995; Radach & Lenhart, 1995). In the ERSEM simulations the physical transport functions as independent hydrodynamic forcing for the ecosystem. Thus there is no feedback from the biology to the hydrodynamics.

Our present understanding of the functioning of the marine ecosystem of the North Sea (and of any shelf sea) as supported by observations and simulations of biological and physical dynamics suggests that the variability of the ecosystem is to a very large extent determined by the variability of the physical environment. Only if the variability of the system is taken into consideration shall we be able to make progress in our understanding of the complexity of the marine ecosystem. The availability of advanced hydrodynamical models provides a sound support for process-oriented ecosystem simulations.

In ERSEM the physical transport of pelagic abiotic and biotic substances is based on physical flow fields simulated by the existing three-dimensional general circulation model for the North Sea elaborated by Pohlmann (1991, 1995a). His model is an extension of the general shelf sea circulation model developed by Backhaus (1983, 1985), based on the primitive shallow water equations. Including temperature as a prognostic state variable, the Pohlmann model is a

three-dimensional baroclinic model. Details of the model setup and of the results are described by Backhaus (1983, 1985, 1989, 1990) and by Pohlmann (1991, 1995a, 1995b).

2. CIRCULATION AND STRATIFICATION OF THE NORTH SEA: GENERAL CHARACTERISTICS AND SPECIFIC SCENARIOS

2.1. SCALES OF THE GOVERNING PHYSICAL PROCESSES

The spatial and temporal scales of the physical environment of the North Sea are governed by the scales of the forcing atmosphere, the tides, the continental freshwater supply and by topography. The North Sea is situated in a meteorologically very active area, the passage of the low pressure cyclones coming from the Atlantic (Becker, 1990). They create high variability in sea state variables such as currents and temperature (Backhaus, 1989). The North Sea basin is large in comparison with the characteristic scales of the atmospheric fields, which are of the order of 10 to 1000 km. Therefore the simulation of its dynamics requires spatially structured atmospheric forcing fields. The time scales of the atmosphere are governed by a very high transient activity, typical of a mid-latitude west wind regime characterized by the so-called synoptic frequency band (3 to 5 days) of the energetic cyclonic activity. Another pronounced frequency band covers the annual cycle. However, an inspection of atmospheric spectra which cover time scales from hours to years does not reveal any low-energy frequency range which could be used to determine a cut-off for a time-averaging or filtering; this has implications for the design of simulations of the long-term variability of the North Sea (Backhaus, 1989).

Systematic model experiments on the variability of the atmospherically induced North Sea dynamics (Backhaus, 1989; Hainbucher *et al.*, 1986, 1987) have revealed that the circulation as well as the stratification reflects, almost directly and solely, the activity of the forcing atmosphere. There is only a marginal inertia in the system due to its thermal stratification which, caused by the existence of a seasonal thermocline, may cover time scales of the order of a few months. The reasons for the fast response to atmospheric disturbances are the shallowness of the sea, the high tidally induced turbulence and, in particular, the lack of the existence of a permanent halocline in the North Sea. Convection, enhanced by increased vertical mixing due to storm action during winter, destabilizes the entire water column; the result is always a complete vertical homogenization of the North Sea water masses. Therefore the baroclinic 'memory' of the North Sea cannot 'remember' any disturbance of its vertical thermo-haline stratification of more than one year ago.

Advected salt anomalies will leave the North Sea basin within a time span of about 3 to 5 years, which is the average basin residence time scale estimated from dispersion simulations and observations of radioactive isotopes (Kautsky, 1985; Backhaus, 1984). Hence, the North Sea cannot 'remember' anomalies in its horizontal, haline stratification for more than about three years. The seasonally varying vertical thermal stratification of the North Sea —with the exception of the Norwegian Trench regime— defines the (local) internal Rossby radius of deformation which typically covers spatial scales of between 5 and 50 km. Mesoscale phenomena such as eddies, fronts, meanders, and other instabilities, have time scales which typically cover some hours up to some days.

The scales of the North Sea tides are characterized by the wavelength of the tidal waves (several hundred km) and by their predominantly semi-diurnal periodicity. The advective excursion during one semidiurnal tidal cycle is in general much less than 50 km. The tides in conjunction with the thermal stratification give rise to frontal systems and 'cold belts' (*e.g.* the German Bight) with typical scales between metres and a few kilometres. The long-term component of the tidally induced dynamics, *i.e.* the tidal residual circulation, is much less energetic than the circulation induced by the lateral stratification of the North Sea. Whereas the tidal residual currents are generally (with only some local exceptions in the Channel) of the order of a few $cm \cdot s^{-1}$, the density-induced circulation may have magnitudes of the order of 10 $cm \cdot s^{-1}$.

2.2. THE LONG-TERM MEAN CHARACTERISTICS OF THE CIRCULATION AND OF THE STRATIFICATION

The North Sea is strongly influenced by the North Atlantic Ocean through the connections to the Atlantic in the north and the English Channel in the south. The depth of the North Sea increases uniformly from south to north. The mean depth of the North Sea is 74 m. It has a volume of 42294 km^3 and a surface area of 573300 km^2 (ICES, 1983). The modified ICES boxes as used in ERSEM have a total volume of 40407 km^3 and a surface area of 513300 km^2.

The ecological importance of the tides lies in the tidally induced turbulent motions causing dispersion, the effect of tidal currents on the bottom, and the tidal residual currents. Maximum tidal speeds range from 20-40 $cm \cdot s^{-1}$ in the open North Sea to 80-140 $cm \cdot s^{-1}$ in coastal areas. The M_2-tide creates three amphidromic points, originating from a propagating Kelvin wave, with tidal heights (amplitudes) of up to 200 cm in coastal areas. The decrease in depth from north to south results in a progressive increase of current speed. Tidal energy is dissipated at the bottom, promoting vertical mixing in the tidal boundary layer. The tidally induced transport processes of advection and mixing are more vigorous in the southern, shallow

parts than in the northern deep parts.

The anticlockwise residual circulation, however, shows velocities of a few $cm \cdot s^{-1}$. There is a preference for cyclonic circulation of the wind-induced currents. The mean annual cycle of water mass transport shows two regimes (see fig. 4 of Backhaus, 1989): the water masses entering from the north turn eastward in the central North Sea and do not reach the continental coastal areas; the southern North Sea is influenced by the Channel inflow. All water masses leave the North Sea via the Norwegian Trench.

Freshwater influences the North Sea in three ways: The most important freshwater input originates from the Baltic and may amount to 1276 $km^3 \cdot a^{-1}$ (Jakobsen, 1986). At times the Baltic outflow may cover large parts of the North Sea (Dickson *et al.*, 1992a, 1992b). The second source is the rivers around the North Sea. The mean annual freshwater input by rivers is about 370 km^3 (Becker, 1990). The influx over the North Sea by precipitation is about 460 km^3 (ICES, 1983). Recent estimates for the North Sea by Damm (pers. comm.) are 559 km^3 for precipitation and 424 km^3 for evaporation, resulting in a net precipitation of 135 km^3. Thus, precipitation and Baltic outflow make up only about 2 to 3% of the total volume of the North Sea, but may locally be of great importance for circulation and stratification.

The mean spatial distribution of salinity is determined mainly by the salty Atlantic inflow and by the freshwater inflow from rivers and the Baltic. A tongue of Atlantic water of salinities >34.75 psu reaches from the north far into the central North Sea and also enters through the Channel from the south. Salinities off less than 34 psu occur in a band of about 50 to 200 km width along the continental and Norwegian coasts. The seasonal variability of salinity is low in most parts of the central and northern North Sea (<0.2 psu), but >1 psu in the continental coastal strip and >5 psu in the Skagerrak (Becker, 1990).

The combination of advective and dispersive transport of water from the coasts and from the ocean is reflected in the salinity structure. Salinity distributions for individual months resemble the long-term average distributions, indicating that long-term water transport dominates over short-term fluctuations. The seasonal variation of horizontal temperature distributions is pronounced. The heat exchange with the atmosphere results in a seasonal reversal of the temperature gradients in coastal areas.

The most important agent for vertical exchange is the heat exchange at the sea surface. During one seasonal cycle the whole of the North Sea loses heat energy, but this results from a composite of sink and source regions; the coastal areas receive energy. The sea surface heat exchange dominates the horizontal heat transport. Surface heating causes seasonal stratification only in deeper parts and for regions of low tidal currents, indicated by the Simpson-Hunter parameter remaining below a certain value. In contrast, for most coastal regions complete vertical mixing will occur. The seasonal warming penetrates only slowly —if at all— into deeper parts of the North Sea, with large vertical gradients in temperature developing over summer. The patterns are jointly determined by the horizontal and the vertical transports, and in shallower regions by the topography.

For further details we refer to atlases (ICES, 1962; Goedecke *et al.*, 1967), the review by Otto *et al.* (1990) and to Backhaus (1989).

2.3. THE VARIABILITY IN THE CIRCULATION

The understanding of oceanographic variability has improved considerably since numerical general circulation models (GCM) allow the systematic investigation of the contributions from different agents to the circulation. For ERSEM we have taken advantage of the simulations performed with the Hamburg Shelf-Ocean Model (HAMSOM) and its variants.

2.3.1. THE HAMBURG SHELF-OCEAN MODEL HAMSOM

The three-dimensional baroclinic general circulation model (GCM) for shelf seas (Backhaus, 1985; Pohlmann, 1991) which provides the hydrodynamical data for the ERSEM model evolved in the early eighties from a vertically integrated two-dimensional storm surge model (Backhaus, 1983). Since then it has been applied to the North Sea dynamics (Backhaus *et al.*, 1991) and to other shelf seas. It was further developed and improved in cooperation with international partners (Stronach *et al.*, 1993), and is now known as the Hamburg shelf-ocean model HAMSOM. The realism of the simulations has been proved by several investigations (Pohlmann *et al.*, 1987; Pohlmann, 1995a).

The basic design of the numerical scheme contains implicit algorithms and second-order schemes for the approximation in the time domain which in their integral effect resulted in very good stability properties and a considerable robustness of the scheme. In particular the implicit components of the model scheme allowed its application for stable long-term simulations which covered simulation periods of several years. For the first time this model provided estimates of the seasonal and interannual variability of the North Sea circulation. This result could be obtained only by implementing the realistic short-term forcing of the atmosphere. These scenarios also served to determine the variability of the concentrations of matter dispersed with the circulation and provided useful input for the discussion about the state of the North Sea environment in view of the threat of anthropogenic pollution (Backhaus, 1990; Backhaus *et al.*, 1986, 1991).

Both the quasi-diagnostic Backhaus and the baroclinic Pohlmann model versions (Backhaus, 1985;

Pohlmann, 1991) are discretized on a grid of approximately 20 km mesh size. The grid uses polar coordinates; the meridional distance is 12', and the longitudinal distance is 20'. The vertical is resolved by 19 layers in the Pohlmann model. The model area comprises the North Sea up to 64° N and 15° W in the Backhaus model version and up to 61° 41' N, 5° 5' W in the Pohlmann model version. Thus Pohlmann's area is smaller, but it also contains the ERSEM boxes.

For ERSEM the results obtained by the two different model versions have been utilized so far:

1. The nonlinear 3-D numerical quasi-diagnostic shelf sea circulation model HAMSOM was integrated over a period of 12 years, from 1970 to 1981. The simulations were driven by actual meteorological data, which were derived from a set of 28-year long time series (1955 to 1982) of six-hourly air pressure fields at the sea level, defined on a 150 km x 150 km grid (Backhaus, 1990; Hainbucher *et al.*, 1986).

2. The scenarios were re-run for the years 1982 to 1992, using the baroclinic version developed by Pohlmann (1991), allowing for the prediction of the temperature fields and thus the development of the thermocline. The circulation model was driven with three-hourly wind stress and air pressure distributions calculated from ship observations (Luthardt, 1987) and by observed sea surface temperature. The model was forced at its northern boundary by sea surface elevation obtained with HAMSOM.

Thus HAMSOM forces the Pohlmann model, and the Pohlmann model results drive ERSEM.

2.3.2. METEOROLOGICALLY INDUCED VARIABILITY OF THE NORTH SEA CIRCULATION

On climatic time scales no long-term trends can be discerned in existing data sets for the physical variables of water discharge, global radiation, wind velocity, temperature, salinity, water masses and stratification (Becker, 1990). For these variables we assume the existence of long-term stationary mean states and variability for the last decades. This is very important to know when considering the observed

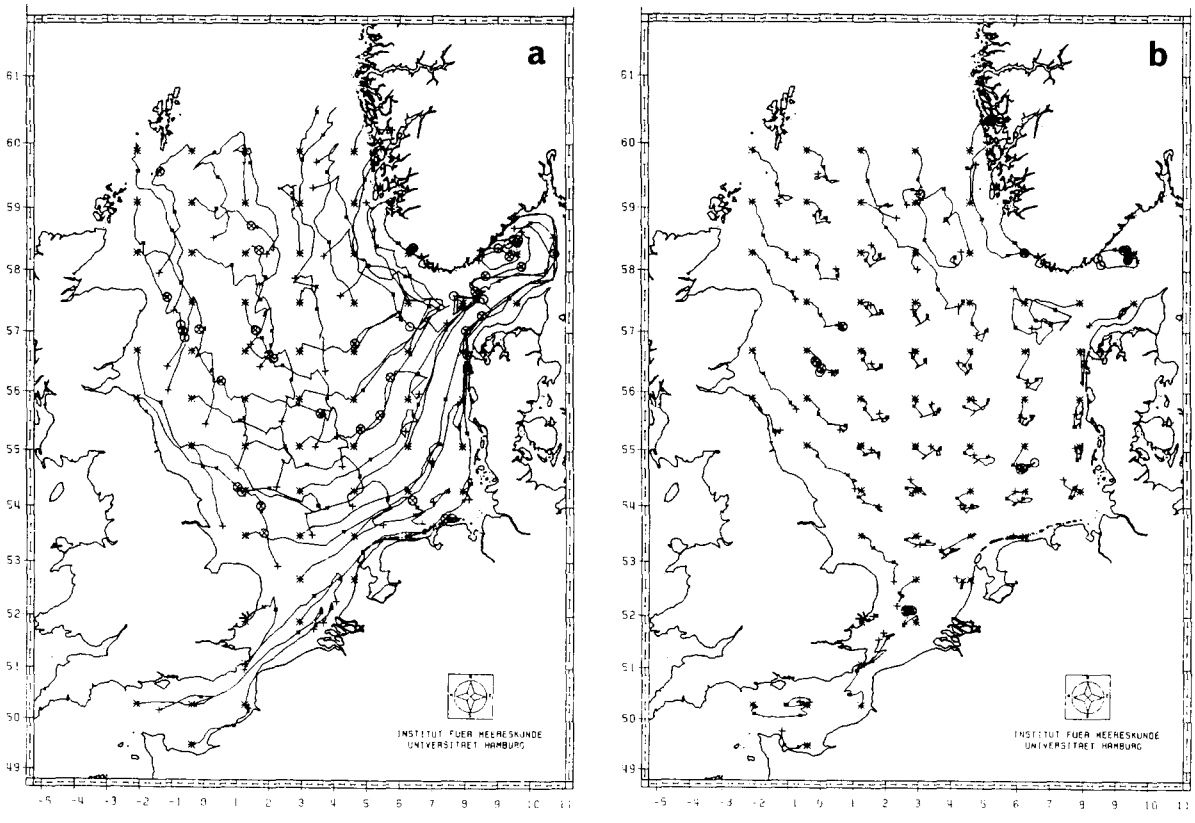

Fig. 1. Flow fields in the North Sea presented by trajectories for 1988 for the layer 0-5 m in a. February; b. April; c. June; d. August; e. October and f. December. The starting and end points are denoted by * and +, respectively. Every ten days a dot is plotted on the trajectories. Upwelling and downwelling are indicated by an encircled dot and x, respectively.

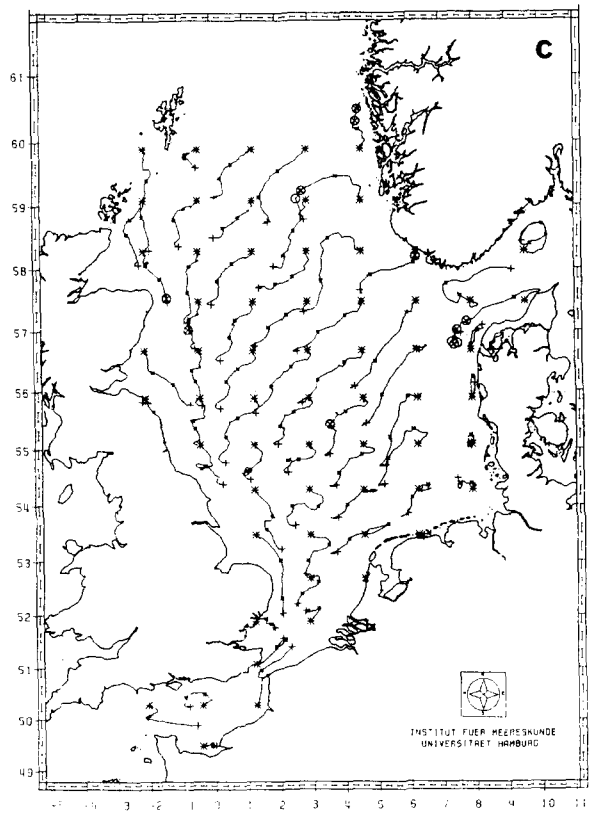
c
INSTITUT FUER MEERESKUNDE
UNIVERSITAET HAMBURG

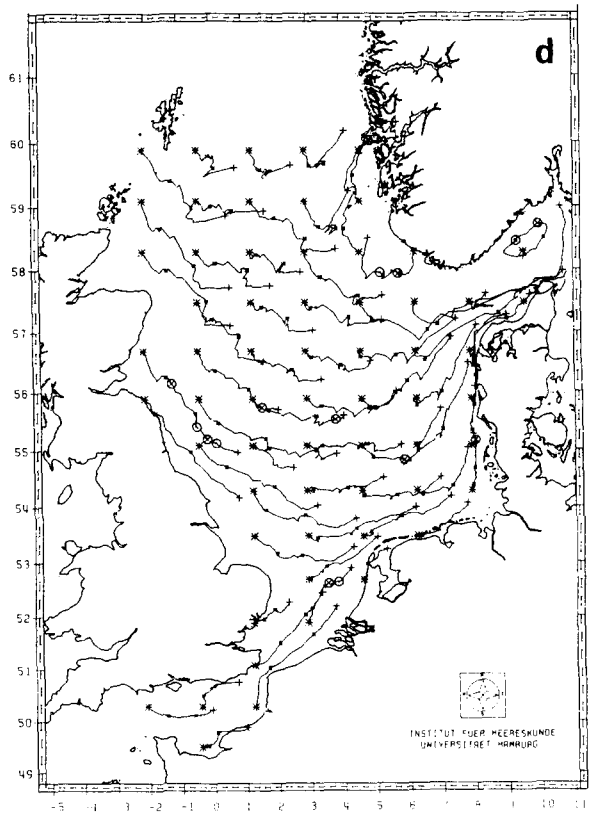
d
INSTITUT FUER MEERESKUNDE
UNIVERSITAET HAMBURG

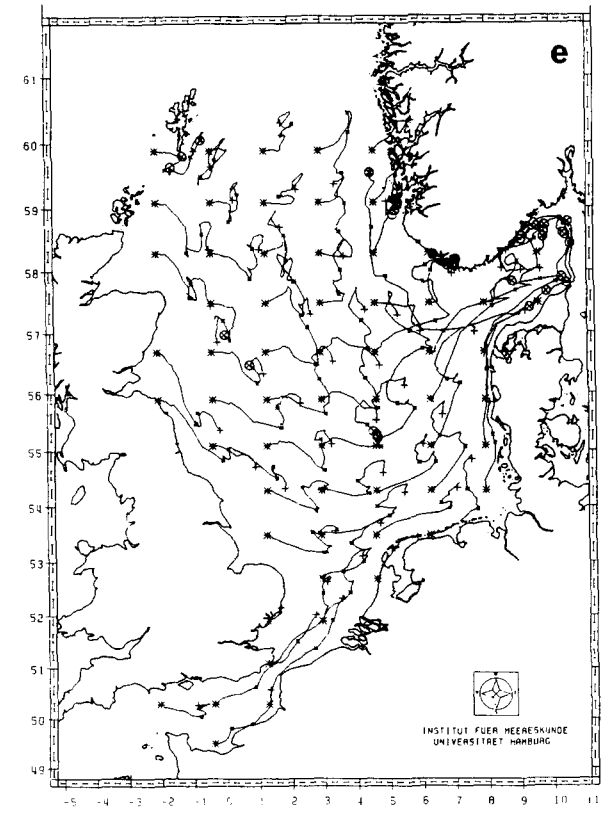
e
INSTITUT FUER MEERESKUNDE
UNIVERSITAET HAMBURG

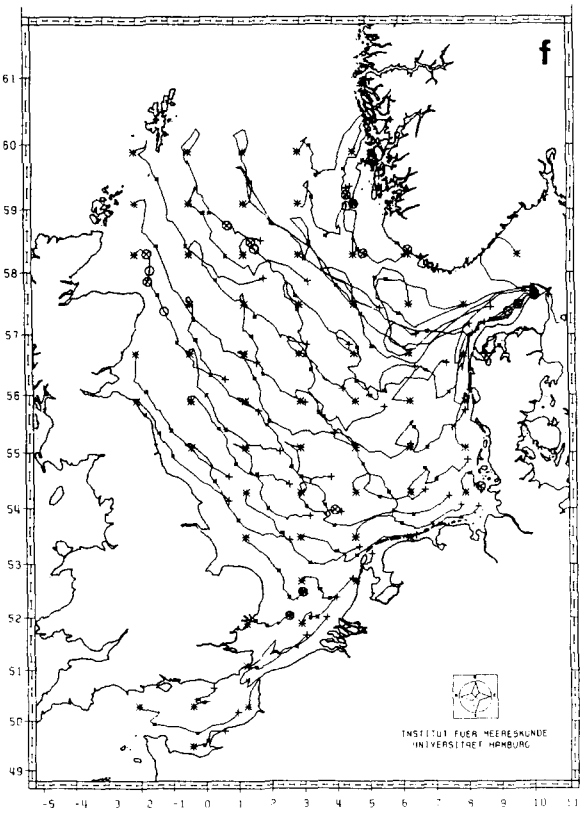
f
INSTITUT FUER MEERESKUNDE
UNIVERSITAET HAMBURG

trends of chemical and biological state variables in the coastal zone (Radach *et al.*, 1986).

The short-term meteorological variability is imposed on the circulation pattern, and both influence the distributions of chemical and biological state variables. The short-term variability is large compared with the means not only for physical, but also for chemical and biological state variables (Radach *et al.*, 1990).

Backhaus *et al.* (1986) and Backhaus (1989) investigated the circulation system of the North Sea by model simulations, taking tides as well as temperature and salinity distributions into account, to obtain information not only about the mean circulation, but also about its fluctuations. They provide quantitative estimates of the relative magnitudes and regional distribution of the contributions of the tide, wind and stratification to the circulation and show the great importance of the fluctuating part of the circulation.

The seasonal variability of the circulation in the North Sea was depicted by means of the transport stream function by Backhaus (see fig. 4 of Backhaus, 1989), showing seasonal means averaged over a simulated ensemble of 12 years. The transports are larger in winter than in summer by a factor of two and exhibit a high degree of high-frequency fluctuations in transport (see fig. 7 of Backhaus, 1989). The variability of the circulation is mainly the result of the variability of the atmospheric forcing fields over the North Sea.

When the mean seasonal forcing fields were derived from the 28-year meteorological data set mentioned above, it could be shown that there is a positive wind stress curl over the North Sea basin, especially during winter, which favours the mean cyclonic circulation (see fig. 1 of Backhaus, 1989). The mean east component of the wind stress during winter is about a factor of three stronger than in summer. The winterly air pressure situation is characterized by a trough between Iceland and the Barents Shelf.

The atmospheric anomalies may yield very different circulation anomalies in the North Sea. Two examples for this were given by Backhaus (see fig. 8 of Backhaus, 1989). In spring 1979 a high pressure cell caused a long-lasting blocking situation. The circulation was reversed and tended to fall apart into a number of eddies. In winter 1974/75 the westerly activity was enhanced by a large-scale low pressure anomaly over the Norwegian Sea, and the cyclonic circulation of the North Sea was enhanced as well.

2.4. THE SCENARIOS SIMULATED BY THE GENERAL SHELF SEA CIRCULATION MODEL

Because the variability in the circulation is of the same order of magnitude as the mean circulation and because we had a large set of validational data for the years 1988 and 1989 from the NERC (Natural Environmental Research Council) North Sea Project and from other sources, we forced ERSEM with GCM simulation results for these years. We chose these scenarios from the available simulations of the circulation over the years 1982 to 1992.

The annual cycle of the circulation system in the North Sea in 1988, as provided by Pohlmann, will be presented as an example by showing the trajectories of water in the surface layer during February, April, June, August, October and December 1988 (Fig. 1).

In February (Fig. 1a) strong currents follow the well-known cyclonic pattern. In the central and southern North Sea we find south-going currents, at least 10 days of the month. The Jutland current enters the Skagerrak in the surface layer, but recirculates in the lower layer. In April (Fig. 1b) the currents are weak all over the North Sea except for some British coastal regions, the Channel area and the very north, where southeast-going currents are observed. In June the pattern is rather different: nearly everywhere southwest-going currents appear except for the British and German/Danish coasts (Fig. 1d). The trajectories in August (Fig. 1c) again map the main transport pattern along the isobaths. This pattern is also dominant in October 1988. The currents are stronger, and the tra-

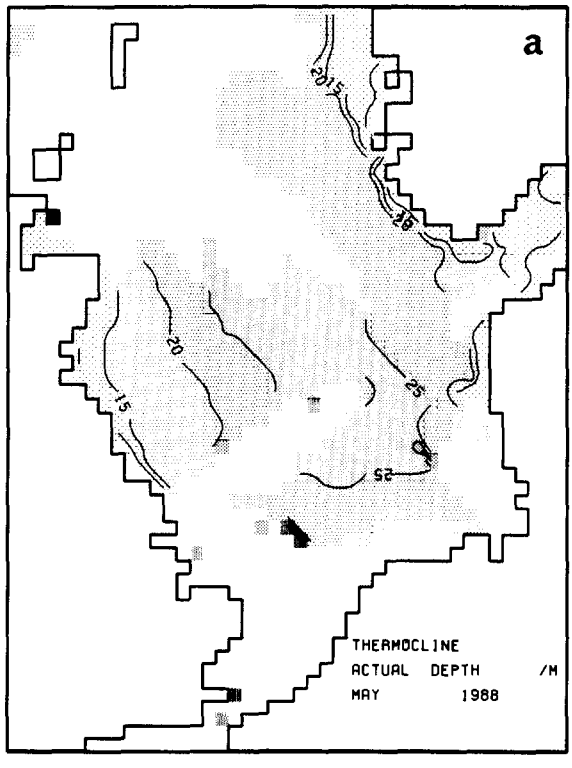

Fig. 2. Mean monthly thermocline depth during May to September (a-e) 1988 from Pohlmann's simulations. The shading changes every 5 m of depth.

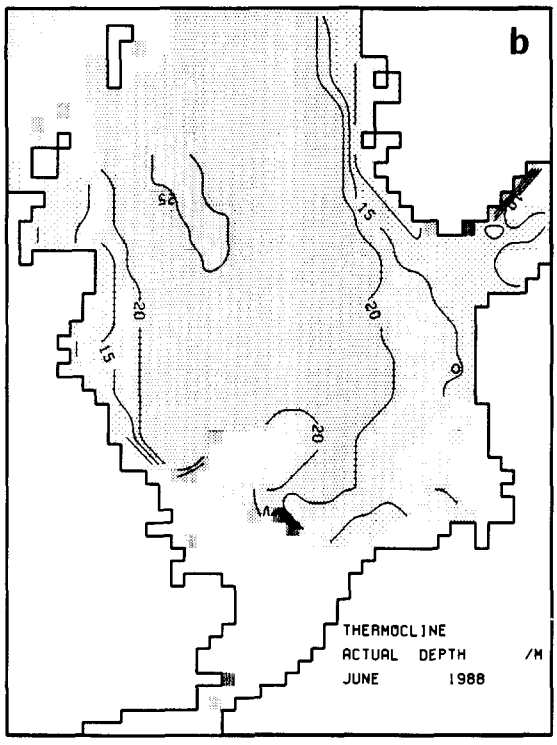
b
THERMOCLINE
ACTUAL DEPTH /M
JUNE 1988

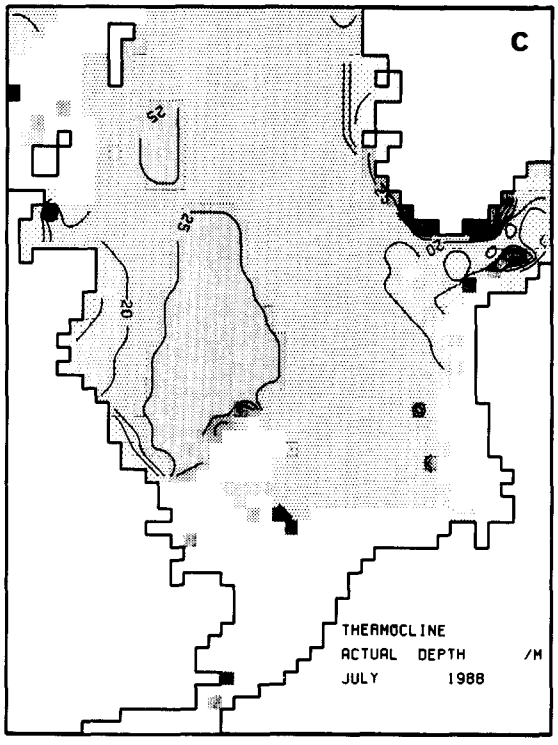
c
THERMOCLINE
ACTUAL DEPTH /M
JULY 1988

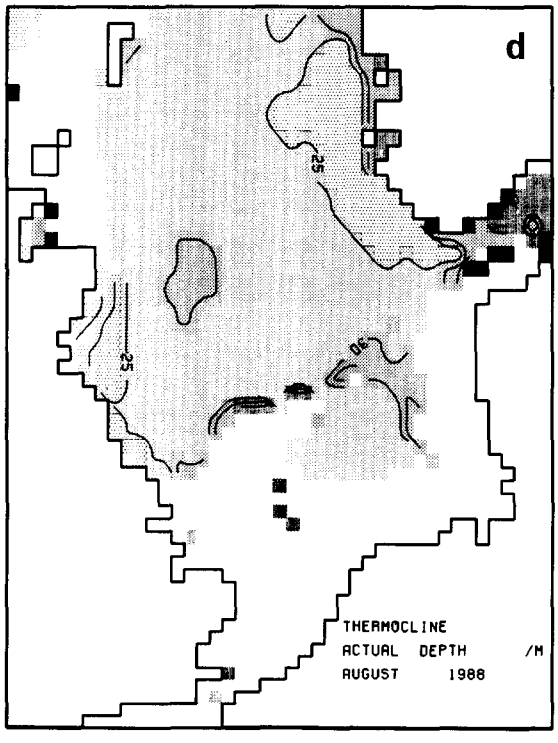
d
THERMOCLINE
ACTUAL DEPTH /M
AUGUST 1988

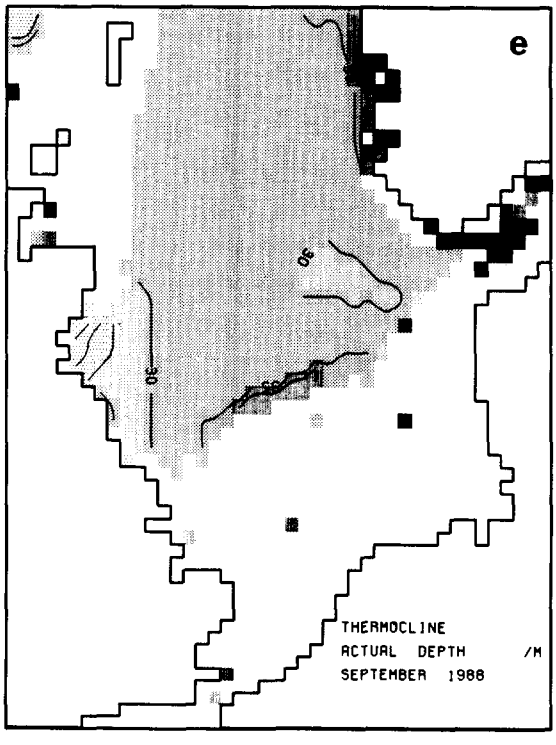
e
THERMOCLINE
ACTUAL DEPTH /M
SEPTEMBER 1988

jectories are partly longer than in August; water is pushed into the Skagerrak, where heavy upwelling occurs (Fig. 1e). The flow in December 1988 is characterized by strong southeast excursions, caused by heavy northwest storms (Fig. 1f). The different patterns of the six months clearly demonstrate the high variability of the currents and that a seasonal or annual mean cannot realistically describe the circulation.

The seasonal thermocline in 1988 as simulated by Pohlmann (1991) lasts from May to September (Fig. 2); it shows shallower depths of 15 to 20 m, when approaching the eastern and western coasts, and 25 to 35 m in the central North Sea. The thermocline is generally deepening from May to September. The regional extension of the simulated mixed layer depth, *e.g.* for May, may also be very different in different years (Fig. 3). The actual depth of the thermocline is as variable as the currents are. In Fig. 3 the thermocline depths are shown for 31 May in 1988 and 1989. While in 1988 the thermocline depth lies between 15 and 30 m, in 1989 the depths are less. The two examples of 1988 and 1989 indicate the range of the lateral and the vertical extent of the mixed layer, derived from prognostic simulations under realistic forcing for a 12-year period. For this simulation the model was thermodynamically driven with observed weekly SSTs. The mixed layer depth range obtained from the 3-D simulation model corresponds well to the mixed layer depths from the 1-D model simulations as performed in the central North Sea (see fig. 7d of Radach & Moll, 1993).

3. THE NORTH SEA WATERFLOW MAPPED ONTO THE ERSEM BOXES

3.1. STRUCTURE AND PROPERTIES OF THE ERSEM BOXES

From the foregoing discussion we can derive minimum requirements for any ecosystem model such as ERSEM, concerning the resolution of scales. The regional differences of the circulation and stratification of the North Sea have to be included at least in the crudest possible way to enable us to represent the regional differences in the chemistry and biology of the North Sea. The solution we adopted was a box model consisting of ten regions, based on the slightly modified division of the North Sea as given by ICES (1983). Because the ICES boxes were defined according to morphological, hydrographic and biological properties of the North Sea, the ERSEM boxes

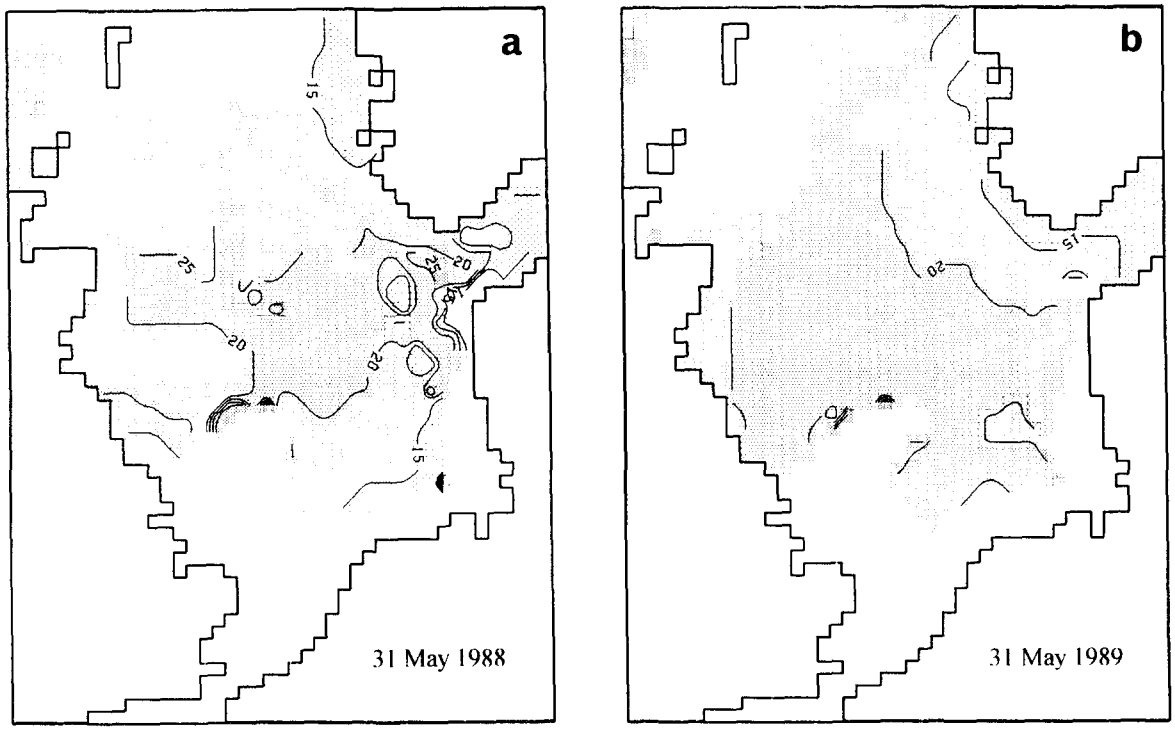

Fig. 3. Thermocline depths for 1988 and 1989, simulated with the baroclinic 3-D circulation model by Pohlmann: a. mixed layer depths during May in 1988 and b. during May 1989.

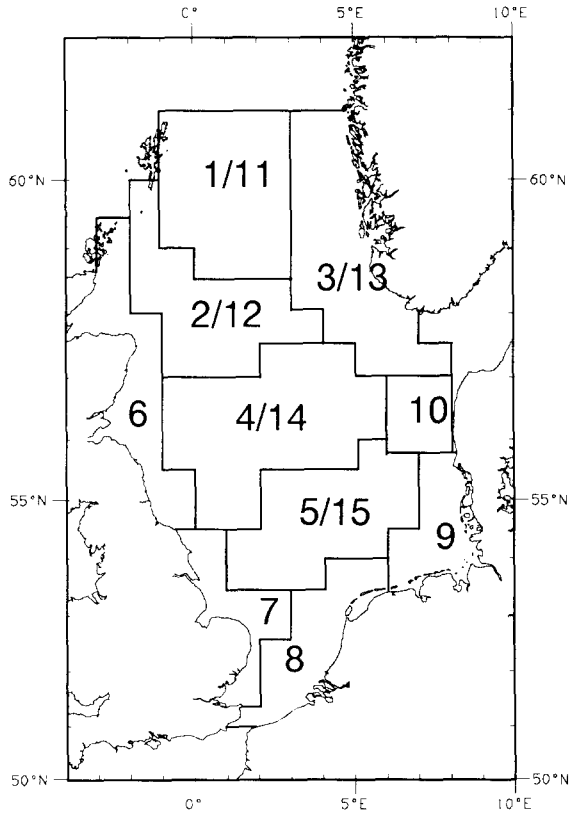

Fig. 4. The horizontal box structure and box numbers of the ERSEM model.

(Fig. 4) provide a crude, but sensible partition of the North Sea.

Another major aspect in the choice of the modified ICES boxes was also, that they are frequently used for presenting aggregated data for the North Sea; for instance they form the structural basis for the North Sea status quality reports (North Sea Task Force, 1993). Therefore the intention was to build the model on a spatial structure which allows an easy data comparison as well as a sensible representation of North Sea subregions.

Since the occurrence of thermal stratification affects the biological development in the water column considerably (Colebrook, 1979; Radach & Moll, 1990, 1993), the boxes of the central and northern North Sea, where thermal stratification occurs regularly, were divided vertically. The average depth of the thermocline, averaged over the North Sea and the season, is about 30 m (see fig. 14.2 of Becker, 1981). The depth of the thermocline varies from south to north within 30 m and during the year at each site from 5 to 30 m (Tomczak & Goedecke, 1962; Pohlmann, 1991). We decided to position the interface between upper and lower layer at 30 m depth for all deep boxes. In Fig. 5 the plane of this horizontal interface is denoted as 'thermocline interface'. The division of the full boxes results in a layer reaching from the surface to 30 m (upper boxes 1 to 5) and a layer from 30 m to the bottom B (lower boxes 11 to 15). The coastal boxes 6 to 10 have no vertical separation. Thus 15 boxes were created in total.

After the definition of the boxes as the spatial scale for the model, the questions have to be discussed what temporal scale should be resolved by the transport forcing and what forcing can be provided by the GCM. The circulation model data set for the North Sea which is defined on a 20-km grid is stored as daily averages. This has two reasons: 1. If the model is run over several years —as was intended—a suitable and practicable data compression is needed; 2. the average Lagrangian excursion of the circulation during one day is usually smaller than the grid size of the oceanographic model (exceptions are extreme excursions during storms); a daily average therefore defines a suitable and well-defined temporal cut-off for the spatial resolution of the model and the dynamics of the North Sea. The daily averaged values stored from the GCM simulations include the daily averaged advective transport in x- and y-directions, the daily variance of the advective transport and the daily averaged vertical diffusion coefficient. The vertical advection, however, has to be calculated by means of the continuity equation from the simulation results.

Since phytoplankton production demands at least daily time increments, the daily averaged transport values by the GCM match the demands of the biological properties of the model quite well. Moreover, the daily variance of the dynamical fields predicted by the model gives a suitable estimate of the subgrid-scale variability of the flow (tides, storms *etc.*). In a three-dimensional transport model (Pohlmann, 1991), based on the GCM results on the 20-km grid, this variance was used to parameterize for instance horizontal turbulent diffusion of matter. Therefore the data available from the GCM model include the potential to parameterize subgrid variability of the flow also for the ERSEM model.

3.2. THE CALCULATION OF THE FLOW THROUGH THE ERSEM BOXES

The GCM flow simulations are based on the grid described in section 2.3.1. The grid determines the detailed location of the box interfaces as illustrated in Fig. 6. The horizontal velocities in eastern and northern directions, u and v, are calculated at grid points shifted by $\frac{1}{2}\Delta x$ and $\frac{1}{2}\Delta y$ to the east and south of the grid points for water level ζ, respectively. The flow across the boundaries of the ERSEM boxes is calcu-

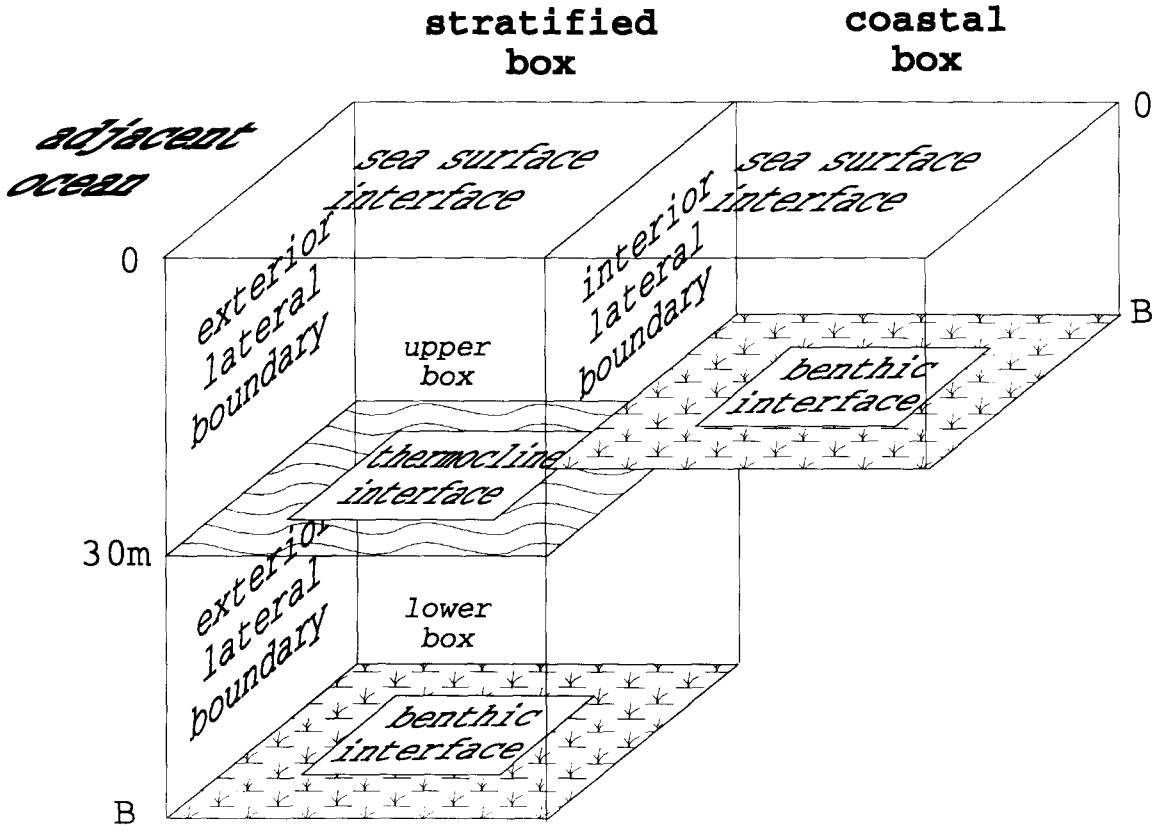

Fig. 5. The internal box structure of the ERSEM model.

lated from the velocity components given on this grid as follows: The east-west boundaries of the boxes are aligned to pass the v-points and the north-south boundaries of the boxes are aligned to pass the u-points of the grid. Then the velocity components are integrated over each of the 50 rectangular ERSEM interfaces to give the flow perpendicular to the interfaces in units of Sverdrups (1 Sv = 10^6 $m^3 \cdot s^{-1}$ = 86.4 $km^3 \cdot d^{-1}$), separately for inflow and outflow. There are 40 internal interfaces between the 15 boxes, 5 of them representing the thermocline as horizontal interfaces. The remaining 10 interfaces act as exterior boundaries towards the adjacent sea areas.

3.3. WATER BUDGET ACROSS THE NORTH SEA BOUNDARIES

Most of the water flow enters the North Sea through the Shetland Channel and the Pentland Firth, and from the Baltic. The largest outflow occurs through the Norwegian Trench. The total inflow (and outflow) varies over the years 1982 to 1992 between about 90000 and about 109000 $km^3 \cdot a^{-1}$, depending on the meteorological situation (Table 1).

Within the 11 years the difference between in- and outflow over the external boundaries of the model area ranges from 0.05 to 0.19% of the actual inflow of the corresponding year. This is much smaller than the error of the water budget of up to 0.5% for the individual ERSEM boxes (Table 2). Therefore the water flow into and out of the ERSEM area is well balanced over one year, even though individual boundaries like the Shetland Channel or the Norwegian Trench show remarkable differences between in- and outflow, which is due to the overall circulation system in the North Sea.

The inflow shows marked seasonal variations, differing between the regions. While the lowest inflow through the Shetland Channel occurs in spring and autumn, maxima often occur in late winter. The inflow through the English Channel is often low during summer and relatively high in autumn and winter. In all time series of inflows very strong events occur from time to time, surpassing the mean by a factor of four or even more. The projection of all annual cycles of inflow into one year shows that the interannual variability is much larger during winter than during summer, especially for the Shetland Channel and the

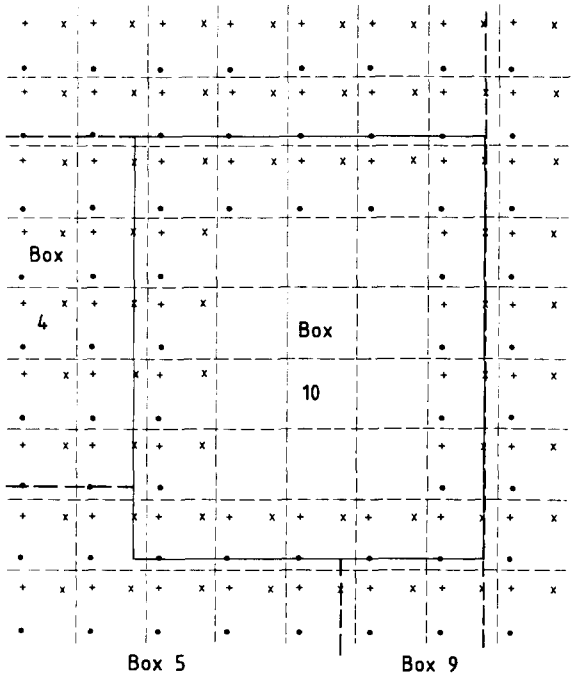

Fig. 6. Matching the computational grid and the ERSEM boxes, *e.g.*, for box 10: + denotes the ζ-point, x indicates the u-point and · the v-point. The vertical box interfaces pass through the velocity points.

Pentland Firth (Fig. 7). The cumulative inflow for the 11 years (1982-1992) is nearly linearly related to time. The variability between the different years is less than 20%.

3.4. WATER BUDGETS FOR THE ERSEM BOXES

The largest inflow and outflow occur at the northern boundary of the North Sea through the deep boxes, except for the Shetland Channel, where both layers transport nearly the same (small) amounts (Figs 8a and 8b). In the northern North Sea about 1.69 Sv or 146 $km^3 \cdot d^{-1}$ of Atlantic water are introduced in the northwest into the boxes 1/11, 2/12 and 6. A large fraction (about 75% to 85%) of these Atlantic water masses sweep across the shelf plateau north of the Dogger Bank to rejoin the Atlantic via the Norwegian trench (box 3/13) at the eastern boundary of the North Sea basin.

TABLE 1

Budgets of water flow into and out of the North Sea over the external boundaries of the ERSEM model area from Pohlmann's simulations for the years 1982 to 1992, in $km^3 \cdot a^{-1}$.

	inflow ($km^3 \cdot a^{-1}$)						
year	*Norw. Trench*	*Shetl. Channel*	*Fair Isle*	*Pentland Firth*	*English Channel*	*Baltic*	*sum*
1982	9871	35132	6700	11209	3480	32491	98883
1983	12640	39227	5935	10231	3125	29768	100926
1984	15366	36795	5080	8709	3213	32463	101630
1985	14670	33270	4468	7753	2989	28375	91948
1986	12982	36619	6304	10968	3380	30880	101556
1987	11962	34420	4998	8494	2734	26744	89775
1988	12864	35703	5373	9252	3569	28339	95100
1989	13640	39986	6689	11338	3056	27553	102517
1990	14357	41304	7066	12049	3673	30727	109452
1991	15347	39659	6248	10690	3175	29170	104565
1992	15421	39802	6219	10853	3015	28729	104040

	outflow ($km^3 \cdot a^{-1}$)						
year	*Norw. Trench*	*Shetl. Channel*	*Fair Isle*	*Pentland Firth*	*English Channel*	*Baltic*	*sum*
1982	59331	6070	1164	1559	1511	29057	98692
1983	62623	5777	1464	1846	1913	27158	100782
1984	61238	7277	1203	1711	1718	28642	101789
1985	55900	6085	1375	1681	1586	24891	91768
1986	63782	5388	1062	1538	1823	27516	101359
1987	54997	6511	1597	1654	1775	22853	89639
1988	58861	6741	1585	1716	1901	24432	95236
1989	66912	6640	1347	1315	1735	24265	102545
1990	70269	6535	1456	1595	1680	27496	109363
1991	67459	6882	1228	1473	1852	25442	104667
1992	68827	5776	1161	1490	1727	25117	104099

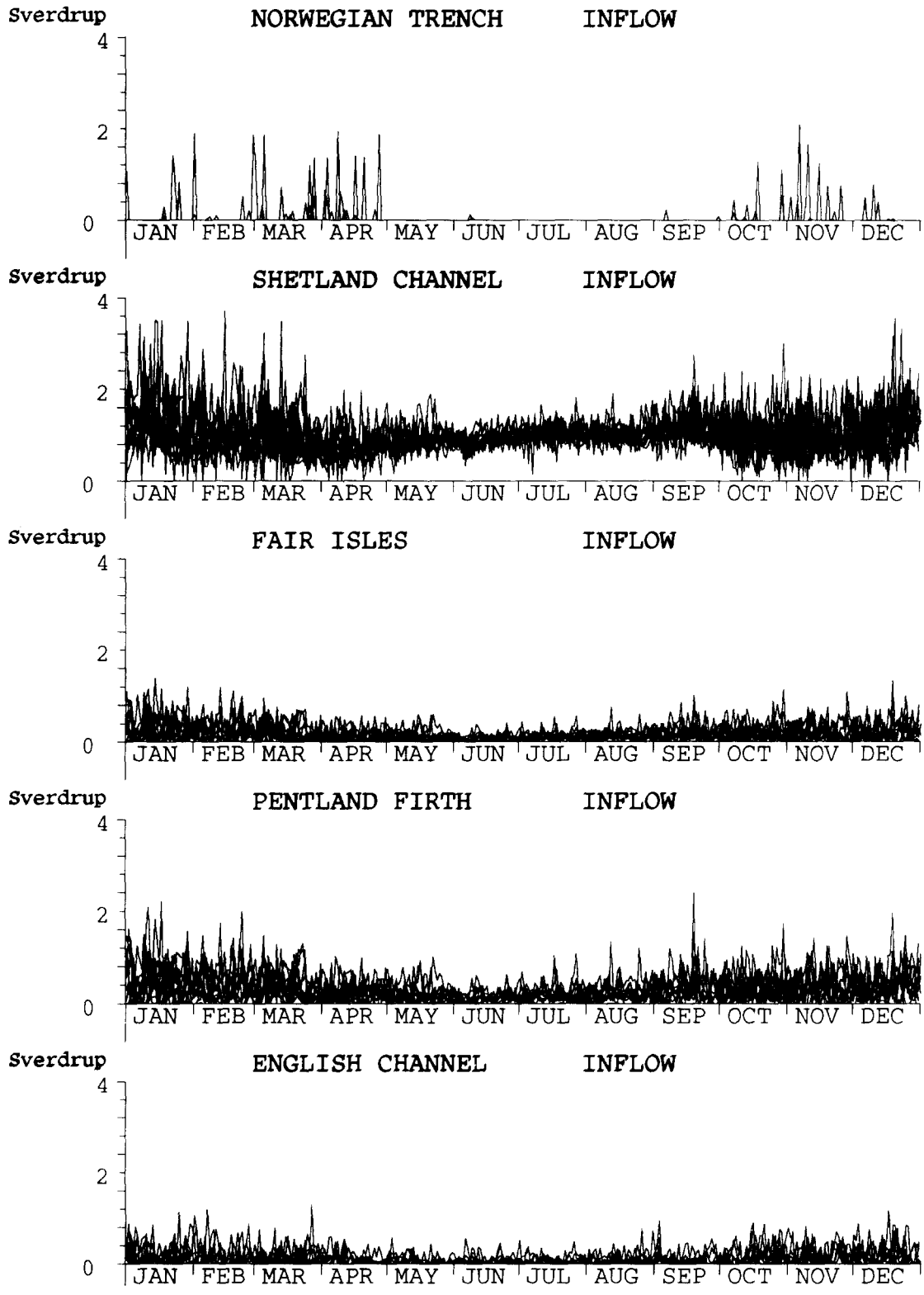

Fig. 7. All 11 annual cycles of simulated net water flows across the external boundaries of the ERSEM region given in Sverdrup, projected into one year. 1 Sv = 10^6 $m^3 \cdot s^{-1}$ = 86.4 $km^3 \cdot d^{-1}$.

Of the remaining Atlantic inflow water some influences the central North Sea, and only a fraction of about 5% contributes to the exchange and flushing of water in the southern parts of the North Sea. The net transport into the southern North Sea occurs mainly through the western part of the central North Sea. Here about 0.08 Sv or 6.9 $km^3 \cdot d^{-1}$ of water join the flow resulting from the flow down along the British coast (box 6) and from the central North Sea (box 4), to flow into box 7. From box 7 only 0.06 Sv finally enter the continental coastal area in box 8. The main source of Atlantic water entering the continental coastal area remains the English Channel with 0.057 Sv inflow into box 8.

Another net contribution from the northern flow regime comes from box 5, which acts as a transition box between the northern and the southern circulation system. From here 0.021 Sv enter the German Bight (box 9). From box 9 as well as from box 5 the water flow joins the recirculation system in the north by their outflow into the Norwegian trench (box 3/13) via the Danish coast (box 10). The outflow of the Jutland current to the Skagerrak in the upper layer reenters the North Sea in the deeper parts of the Norwegian Trench (box 3), masking the relatively small Baltic outflow in the upper layer and the Baltic inflow in the lower layer. For the stratified boxes 1/11 to 5/15 the vertical water exchange is presented in Figs 8a and 8b by open arrows, showing up- or downwards flow into or out of the upper boxes 1 to 5. For boxes 1 and 2 the net flow is directed into the upper boxes; these boxes also have the highest of all vertical flows of water of 0.66 and 0.46 Sv, respectively. The other stratified boxes have a net flow of between 0.264 and 0.02 Sv into the lower boxes. Compensatory vertical flow is substantial in boxes 1, 2 and 3, and it is of

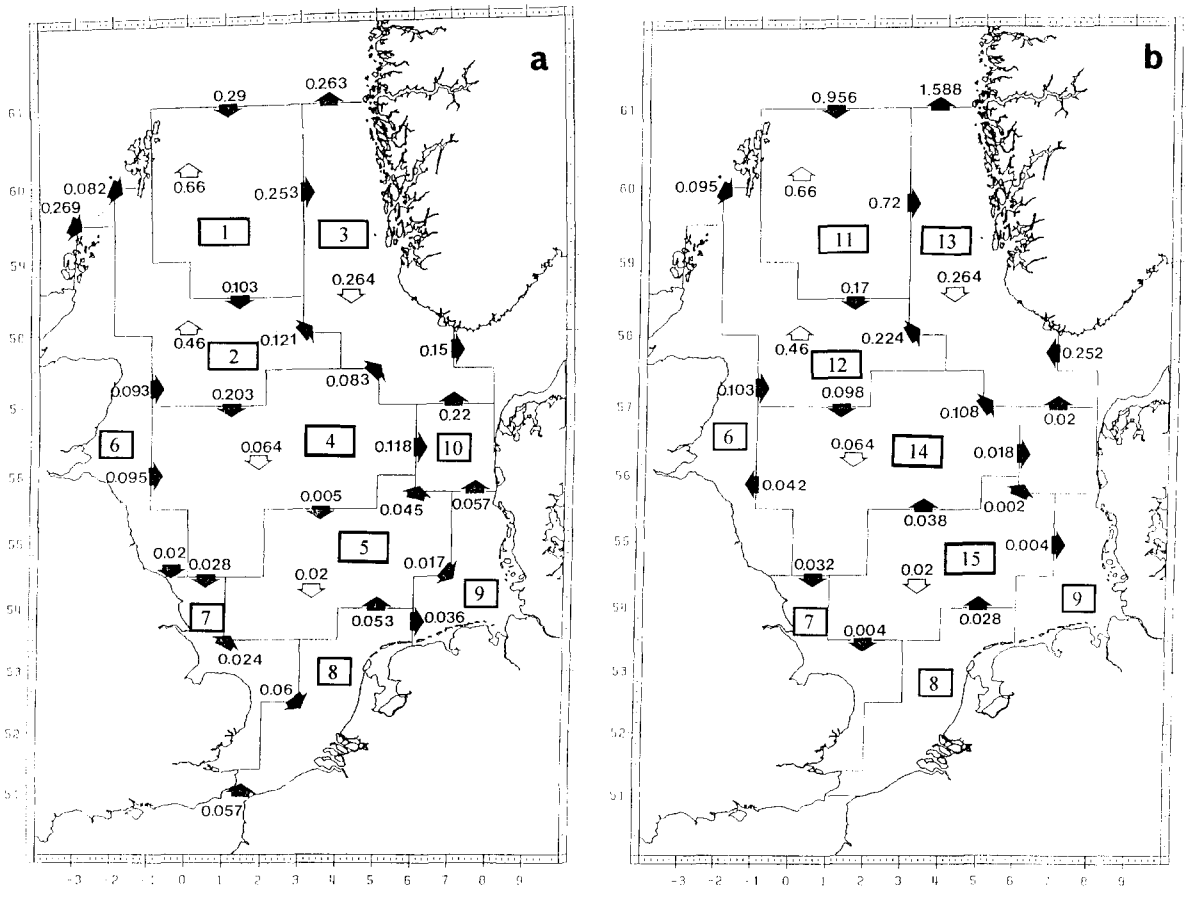

Fig. 8. Mean net flows (1982 to 1992) through the boundaries of a. upper and b. lower ERSEM boxes, in Sverdrup. The open arrows indicate the vertical transport between upper and lower boxes.

minor importance in boxes 4 and 5.

In Table 2 the water budget for the overall boxes from the surface to the bottom is presented for 1988 and 1989. For both years the budgets are well balanced. Calculating the net difference between in- and outflow as percentage of the inflow for each box yields values of between 0.011 and 0.241% for 1988 and between 0.018 and 0.214% for 1989. The two years of simulation results from the Pohlmann model reflect the strong variability of the wind forcing on the circulation model (Pohlmann, 1991).

Box 3 shows by far the highest values of in- and outflow. This corresponds to the well-known circulation pattern where the Norwegian Trench region combines water from the northern and southern circulation systems forming the main outflow for the North Sea. Within boxes 1 and 2 strong in- and outflows can be observed in relation to the Atlantic inflow in the north. The German Bight box 9 clearly has the lowest values, whereas the much smaller Danish coastal box 10 reaches twice the values of box 9. This agrees with the fact that the Danish coastal box 10 represents a major outflow for the southern circulation system into the Norwegian Trench box 3. The values in boxes 4 and 5, areas of the central North Sea, exceed those for box 8, the Dutch coastal box with the inflow of the English Channel, as well as those for box 6, the Scottish coastal box with an open boundary towards the North Atlantic.

In addition to the values of the specific years, the ranges of minima and maxima of in- and outflows within the period 1982 to 1992 is given in Table 2. Here the values for in- and outflow do not necessarily originate from the same year. The values for the two years of interest for the ERSEM simulations are well within the range of values observed during the 11 years and do not constitute extreme situations.

3.5. FLUSHING TIMES

The flushing times are calculated by dividing the total volume of a box by the total inflow into the box V_g / Q^i. Since the concept of flushing times was introduced along with the division of the North Sea into the ICES boxes (ICES, 1983), these boxes form the basis for the comparison of different flushing time calculations. Using the ERSEM boxes this implies that no vertical separation is applied for the northern and central boxes and that the volume always refers to the total box volume V_g. In Table 3 estimates for the flushing times from different investigations are summarized.

The flushing times calculated within ERSEM exhibit a clear seasonal signal with the shortest flushing times in winter. Even for box 10, which has by far the shortest flushing times of between 2 and 28 days, this seasonality can be observed. Box 10 is exceptional, because the box has the smallest volume (404 km^3) and acts as a transition box for the water flow from the southern circulation system into the Norwegian Trench. The exchange times of all the boxes lie between 2 (box 10) and 75 (box 6) days. The water masses of the German Bight (box 9), for instance, are exchanged within an average of 32 days in winter, and flushing times range from 11 to 58 days. The variability of the flushing for each box is considerable. The deep Norwegian Trench box (ERSEM boxes 3 and 13) may be flushed within 19 days (minimum) to 49 days (maximum).

Lenhart (1990) calculated flushing times based on data from the Backhaus (1985) model simulations for the years 1970 to 1981. Generally the values for the flushing times correspond to ERSEM calculations, especially for boxes 5 and 10. However, the different years under consideration and the improved model version by Pohlmann (1991, 1995a, 1995b) lead to larger ranges for most of the boxes, which can be

TABLE 2

Cumulative inflow and outflow for all boxes for 1988 and 1989, and ranges for the 11 years (1982 to 1992) from Pohlmann's simulations, in $km^3 \cdot a^{-1}$.

ERSEM	*1988*		*1989*		*1982-1992*			
	in	*out*	*in*	*out*	*range in*		*range out*	
box					*min*	*max*	*min*	*max*
1 + 11	65966.	66063.	68134.	68213.	59155.	71132.	59200.	71214.
2 + 12	68112.	68148.	67049.	67064.	57323.	72622.	57314.	72620.
3 + 13	123349.	123251.	129379.	129206.	112709.	139058.	112591.	138888.
4 + 14	59560.	59617.	54819.	54863.	49897.	61387.	49926.	61395.
5 + 15	32407.	32402.	28135.	28129.	26686.	32407.	26679.	32402.
6	26831.	26896.	27781.	27824.	23524.	30995.	23560.	31018.
7	15238.	15243.	12817.	12826.	12412.	15238.	12437.	15243.
8	19209.	19204.	15604.	15591.	15429.	19209.	15438.	19204.
9	7386.	7385.	6299.	6284.	5793.	7539.	5798.	7513.
10	14191.	14180.	12345.	12335.	11475.	14611.	11466.	14599.

TABLE 3

Maximum, minimum and the mean values of flushing times calculated by using the box volumes of the ERSEM boxes and the advective inflow as applied in the ERSEM model, in comparison with calculations by Backhaus (1984) and by Lenhart (1990). The values for box 9 marked by * from the Backhaus calculations indicate that these flushing times were calculated for the volume and inflow of the combined boxes 9 and 10.

ERSEM					*Lenhart (1990)*			*Backhaus (1984)*	
box	*volume*	*min*	*max*	*mean*	*min*	*max*	*mean*	*min*	*max*
	(km^3)		*(d)*			*(d)*		*(d)*	
1+11	6345	20	48	35	27	54	41	35	48
2+12	5644	14	56	31	18	37	28	9	39
3+13	12815	19	49	37	33	60	47	41	61
4+14	6190	19	66	40	25	54	38	32	49
5+15	2770	12	53	33	16	48	30	31	39
6	3176	19	75	42	19	50	33	13	41
7	1138	11	51	30	11	37	21	15	30
8	1323	8	49	28	8	40	19	21	29
9	602	11	58	32	9	49	26	10*	27*
10	404	2	28	11	3	25	10		

seen in the shift of the mean value as well as in a shift of the range between the minimum and maximum values. For the ERSEM boxes 2 and 4 to 9 higher mean values coincide with a shift of the maxima to higher values. For boxes 1 and 3, however, a shift to lower values can be observed. In box 3 the range between minimum and maximum has widened resulting in a higher mean value.

Table 3 also gives data on flushing times from a simulation lasting for six months (Backhaus, 1984) as minimum and maximum values. These data are well within the range given by the flushing times resulting from the ERSEM calculations, except for the minimum value of 9 days for box 2 and the maximum value of 39 days for box 2. The minimum value of 9 days is much lower than the corresponding value of 14 days for the ERSEM box 2. This is surprising, since the Backhaus (1984) calculations covered the summer period, when a reduced circulation tends to lower the inflow values and therefore gives larger flushing times.

3.6. VERTICAL DIFFUSION

In addition to the water flow also the vertical diffusion coefficients were calculated from the hydrodynamical model output as mean diffusion values over all grid cells lying on the interface between upper and lower boxes at 30 m as daily time series.

Fig. 9 shows the vertical diffusion coefficients at the five thermocline interfaces between the boxes, for boxes 1/11 to boxes 5/15, for 1988 and 1989. The vertical diffusion coefficients range from 50 to 600 $cm^2 \cdot s^{-1}$ from September to March or April in 1988. They drop to near zero during the stratification period from May to September. The overall pattern is similar between the two years, even though the daily variability within the time series is considerable. Single events may differ strongly. For instance a peak occurs in the vertical diffusion coefficients at the end of February and the beginning of March 1988 which can be seen for all interfaces, but which does not occur in 1989. Box 5 shows a different behaviour with higher values prevailing during the summer periods. This reflects the shallowness of the sea area with a mean depth of around 40 m, where bottom friction influences the vertical diffusion values at the 30-m interface.

4. THE ADAPTATION OF THE FLOW FIELDS TO THE ERSEM BOX MODEL

In this section the rationale of deriving the box model equations from the transport equation is outlined and the adaptation procedure for introducing the forcing time series into the box model is presented. Furthermore flow adjustments arising from intrinsic problems of this adaptation will be discussed.

4.1. THE GENERAL BOX MODEL EQUATIONS

Box model equations have been presented in many papers (see *e.g.* Uncles, 1988). Mostly discretized versions of the equations are presented (see *e.g.* Baretta & Ruardij, 1988). Keeling & Bolin (1967) derive box model equations from the transport equation for a concentration C of a substance, including the presentation of parameterizations of all turbulent fluxes. They, however, used the equations for determining the flows inversely from known concentration measurements. As ERSEM is used as a prognostic tool, the derivation of the equations had to be modified, especially because fine-scale water flows were to be included.

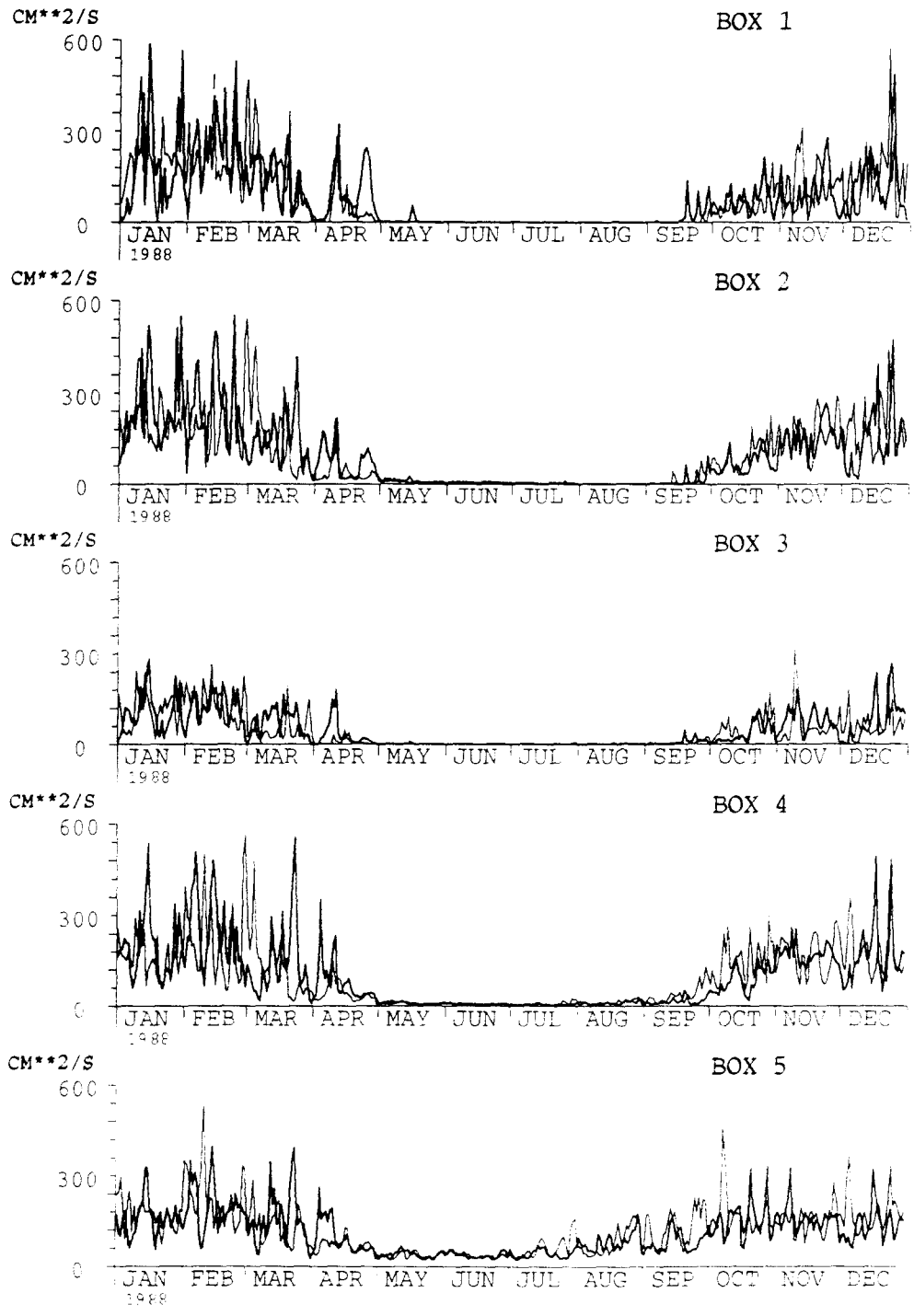

Fig. 9. Annual time series of daily vertical diffusion coefficients, at the thermocline interface for the five vertically separated boxes in $m^2 \cdot s^{-1}$ for 1988 (thick line) and 1989 (thin line). From Pohlmann (1995b).

In the following a modified version of the general box model equation, derived from the general transport equation for any pelagic state variable, is used which is adapted to the forcing taken from the 3-D circulation simulation, thereby keeping the transport equation in a form with physically interpretable terms of advection and diffusion (Radach, 1994). In a second step we will write down the theoretical formulations in accordance with the ERSEM notation conventions and documentation.

The formal derivation of the general box model equation concerning the transport terms for a substance concentration $\bar{C}_i$ within a surface box i of the volume V_i (Radach, 1994) yields the general form

$$\frac{\partial \bar{C}_i}{\partial t} + \underbrace{\frac{1}{V_i}\sum_{j=x}^{-z} F_{ij}\left\{\bar{C}_{ij}\left[\bar{v}_j^{+}\right]_{ij} - \bar{C}_{ij}\left[\bar{v}_j^{-}\right]_{ij}\right\}}_{\text{advection}} + \underbrace{\frac{1}{V_i}F_{iz}\bar{C}_i\frac{\partial \zeta_i}{\partial t}}_{\text{sea level change}} - \underbrace{\frac{1}{V_i}\sum_{j=x}^{-z} F_{ij}K_{ij}^{*}\frac{\Delta \bar{C}_{ij}}{\Delta r_i}}_{\text{turb. diffusion}} - \underbrace{F_{iz}S(t)}_{\text{surface flux}} = \underbrace{[R]_i}_{\text{reactions}} \qquad (1)$$

where the single terms are not yet parameterized in terms of box model state variables. The overbar denotes daily averaging. The second term on the left-hand side

$$\frac{1}{V_i}\sum_{j=x}^{-z} F_{ij}\left\{\bar{C}_{ij}\left[\bar{v}_j^{+}\right]_{ij} - \bar{C}_{ij}\left[\bar{v}_j^{-}\right]_{ij}\right\}$$

sums up all the advective transport through the four vertical interfaces F_{ij} (j=x,-x,y,-y) plus the one through the horizontal interface j=-z at the bottom of the box (for details see Radach, 1994), named thermocline interface in the ERSEM box setup shown in Fig. 5 for a surface box. $\bar{C}_{ij}$ describes the substance concentration on the interface F_{ij}, whereas $\left[\bar{v}_j^{+}\right]_{ij}$ denotes the positive part of the current vector component j averaged over the interface F_{ij} and $\left[\bar{v}_j^{-}\right]_{ij}$ the negative part. The third term

$$\frac{1}{V_i}F_{iz}\bar{C}_i\frac{\partial \zeta_i}{\partial t}$$

describes the change in concentration $\bar{C}_i$ caused by the change of the surface elevation ζ. In the formulation of the ERSEM box model the volumes are assumed to be constant. Therefore the third term for a varying sea surface ζ vanishes. Like the second term for the horizontal advective transport the fourth term

$$\frac{1}{V_i}\sum_{j=x}^{-z} F_{ij}K_{ij}^{*}\frac{\Delta \bar{C}_{ij}}{\Delta r_i}$$

sums up the diffusive transport through the four vertical interfaces plus the horizontal one at the bottom of the box (j=-z). Here K^{*}_{ij} denotes the diffusivities, $\Delta \bar{C}_{ij}$ the horizontal or vertical gradient of the concentration and Δr_i the horizontal or vertical scale of the concentration gradient on the interface F_{ij}.

The term $F_{iz}\,S\,(t)$ describes the flux at the sea surface, if we allow for atmospheric input $S\,(t)$ per unit area and time of a substance C. Since we do not assume any flux across the air-sea interface in the present version of the ERSEM model, the turbulent flux at the sea surface also vanishes. Finally the term on the right-hand side $[R]_i$ represents the temporally and spatially averaged source and sink terms over volume V_i of box i.

We neglect horizontal diffusion (see section 4.4.) and keep only vertical diffusion at the 30 m interface. Therefore only the component j=-z remains. Choosing parameterizations for all terms involving concentrations $\bar{C}_{ij}$ on interfaces (for details see Radach, 1994) Eq. 1 becomes, spelling out all the terms on the interfaces F_{ij}, for j=x,-x,y,-y,-z:

$$\begin{aligned}\frac{\partial \bar{C}_i}{\partial t} + \frac{1}{V_i}\Big\{ & F_{ix}\left(\bar{C}_i\left[v_1^{+}\right]_{ix} - \bar{C}_x\left[\bar{v}_1^{-}\right]_{ix}\right) - F_{i-x}\left(\bar{C}_i\left[\bar{v}_1^{+}\right]_{i-x} - \bar{C}_{-x}\left[v_1^{-}\right]_{i-x}\right) + F_{iy}\left(\bar{C}_i\left[v_2^{+}\right]_{iy} - \bar{C}_y\left[\bar{v}_2^{-}\right]_{iy}\right) \\ & - F_{i-y}\left(\bar{C}_i\left[v_2^{+}\right]_{i-y} - \bar{C}_{-y}\left[\bar{v}_2^{-}\right]_{i-y}\right) + F_{i-z}\left(\bar{C}_i\left[v_3^{+}\right]_{i-z} - \bar{C}_{-z}\left[\bar{v}_3^{-}\right]_{i-z}\right)\Big\} - \frac{1}{V_i}F_{i-z}K^{*}{}_{i-z}\cdot\frac{\Delta \bar{C}_{i-z}}{\Delta r_i} - \frac{1}{V_i}F_{i-z} \\ & = [R]_i \end{aligned} \qquad (2)$$

In the model code for ERSEM the horizontal advective inflows and outflows of the substance $\bar{C}$ will be summed up for the interfaces between the boxes i and j=(-x,-y,x,y) to give the advective transport terms denoted by *whiC* and *whoC*, respectively, following the ERSEM conventions. When considering a surface box, the vertical advective transports denoted by *wviC* and *wvoC* correspond in the following to the formulation for the interface between the boxes i and j=-z . The last term on the left-hand side gives the vertical diffusive transport, denoted by *wdiC* or *wdoC*, for the same interface as the vertical advective transport.

From Pohlmann's model runs horizontal and vertical velocities $\bar{v}_j^+$, $\bar{v}_j^-$ and vertical diffusivities K_{i-z}^* at the 30 m interface were provided to be utilized in ERSEM according to Eq. 2.

4.2. THE SETUP OF THE ERSEM BOX MODEL

4.2.1. ERSEM BOX MODEL CONSERVATION EQUATION

In the present form of the daily integrated flow the horizontal flow components represented in ERSEM are restricted to the horizontal advective parts of the flow, while the vertical transports consist of a diffusive and an advective share. Following the code conventions for ERSEM, Eq. 2 was rewritten as

$$\frac{dC}{dt} = whiC - whoC + wviC - wvoC + wdiC - wdoC + wriC + \text{reaction terms} \quad (3)$$

where the contributions to the concentration change are now summed according to their (positive or negative) effect on the concentration; all biological terms are summarized as reaction terms;

whxC : horizontal advective transport
wvxC : vertical advective transport between adjacent layers
wdxC : vertical diffusive transport between adjacent boxes
wriC : riverine input

In these abbreviations x can denote either inflow (=*i*) or outflow (=*o*). The reaction terms indicate the additional contributions by chemical and biological processes from other submodels, such as the benthos model, the primary production model *etc.*, which also contribute to the changes within the pelagic system.

4.2.2. HORIZONTAL ADVECTION

The contribution of the horizontal advective transport into the box to the change of C is given by all inward transports within the brackets in Eq. 2, reading now in the ERSEM notation as

$$whiC = \frac{1}{V}\sum_{j=1}^{N} U_j^i \cdot F_j \cdot C_j \quad (4)$$

with:

N : number of lateral boundary areas F_j for the adjacent box j
F_j : lateral boundary area j to the adjacent box j
U^i_j : flow into the box through the area F_j, given by Pohlmann's model simulation integrated over one day
C_j : concentration in the outer box j adjacent to area F_j
V : volume of the box

The contribution of the horizontal transport out of the box to the change of the concentration C is given by:

$$whoC = \frac{1}{V}\sum_{j=1}^{N} U_j^o F_j C \quad (5)$$

with:

U^o_j : flow out of the box through the area F_j, given by Pohlmann's model simulation, integrated over one day
C : concentration of the substance in the box

4.2.3. VERTICAL ADVECTION

The vertical advective velocity is not calculated explicitly by the GCM, and we have to compute vertical advection from the horizontal flows by means of the continuity equation. When introducing a thermocline interface, the inflow and outflow of each of the separate layers do not necessarily balance, because these may occur either vertical advection or surface height changes, or both. Therefore, we have to consider whether vertical advective transport through this interface alone can compensate for such an imbalance. Since information is only available for the total horizontal advective transport, the vertical advective transport has to be calculated from the resulting horizontal inflow and outflow in each of the upper and lower boxes separately.

Denoting with Q for volume flows, V for volumes and with the indices u for upper boxes, l for lower boxes, t for total (upper plus lower) boxes, i for inflows into the box, o for outflows out of the box, v for vertical flows (positive downwards), we now give the detailed formulae used in ERSEM. The first step is to calculate the net flow ΔQ for the upper and lower boxes as inflow Q^i minus outflow Q^o. In addition, a total net flow ΔQ_t is calculated for the overall box (upper plus lower subboxes) with the volume $V_t = V_u + V_l$:

$$\Delta Q_u = Q_u^i - Q_u^o \quad (6)$$

$$\Delta Q_l = Q_l^i - Q_l^o \quad (7)$$

$$\Delta Q_t = \Delta Q_u - \Delta Q_l \quad (8)$$

If there were no net vertical flows, then

$$\Delta Q_u = \Delta Q_l = \Delta Q_t = 0 \quad (9)$$

While ΔQ_u and ΔQ_l may amount to significant percentages of the inflow into the layer, ΔQ_t is only a small percentage of Q_t.

From continuity the differences ΔQ_u and ΔQ_l equal the vertically advected amount of water Q^v

$$\Delta Q_u = Q^v \quad (10)$$

$$\Delta Q_l = -Q^v \quad (11)$$

This would be fully correct if there was no effect of water level change. The small deviation ΔQ_t equals the amount of water transported due to water level change, which is not accounted for in the present ERSEM. To include the effect of vertical motions on the chemical and biotic constituents induced by water level changes without using the full equations for a free surface, we artificially modify the vertical advection a little by distributing ΔQ_t over the upper and lower boxes according to their volumes, defining

$$\Delta Q_u^* = \Delta Q_t \frac{V_u}{V_t} \quad (12)$$

$$\Delta Q_l^* = \Delta Q_t \frac{V_l}{V_t} \quad (13)$$

and assuming

$$Q_u^v = \Delta Q_u - \Delta Q_u^* \quad (14)$$

$$-Q_l^v = \Delta Q_l - \Delta Q_l^* \quad (15)$$

Then

$$Q_u^v = Q_l^v \quad (16)$$

The consequence is that the water budgets for the upper and lower layers are now erroneous by the small amounts

$\Delta Q_t \frac{V_u}{V_t}$ and $\Delta Q_t \frac{V_l}{V_t}$ respectively.

For adjusting the flow to exact fulfilment of continuity also in the present box model version, a linear optimization scheme is used to minimally redistribute the flows (see section 4.3.). In order to introduce the vertical transport into Eq. 3 we now define $wviC$ and $wvoC$, depending on the sign of $Q_u^v = Q_l^v = Q_v$:

If $Q_v < 0$, *i.e.* for upward transport

$$(wviC)_u = \frac{1}{V_u} Q_v \cdot C_l \,,\ (wviC)_l = 0$$
$$(wvoC)_u = 0 \,,\ (wvoC)_l = \frac{1}{V_l} Q_v \cdot C_l \quad (17)$$

If $Q_v > 0$, *i.e.* for downward transport

$$(wviC)_u = 0 \,,\ (wviC)_l = \frac{1}{V_l} Q_v \cdot C_u$$
$$(wvoC)_u = \frac{1}{V_u} Q_v \cdot C_u \,,\ (wvoC)_l = 0 \quad (18)$$

4.2.4. VERTICAL DIFFUSION

Vertical diffusion appears in the box model only at the 30-m thermocline interface. However, in nature the thermocline is not a mathematical plane, but has a certain thickness. According to observations this varies from 5 to 40 m. The summer mean value of the thickness is about 20 m (Soetje & Huber, 1980). This value has been taken as the length scale L for vertical turbulent diffusion. Since the difference in the concentration of a substance between upper and lower box enters the calculation (see last term in Eq. 2), net diffusion is only acting into or out of a box at each time step. For the upper boxes (1 to 5) net diffusion is calculated according to:

If $C_l > C_u$:

$$(wdiC)_u = -\frac{1}{V_u}\left(D_v \frac{C_u - C_l}{L}\right)F \,,\ (wdiC)_l = 0$$
$$(wdoC)_u = 0 \,,\ (wdoC)_l = \frac{1}{V_l}\left(D_v \frac{C_l - C_u}{L}\right)F \quad (19)$$

If $C_l < C_u$:

$$(wdiC)_u = 0 \,,\ (wdiC)_l = \frac{1}{V_l}\left(D_v \frac{C_l - C_u}{L}\right)F$$
$$(wdoC)_u = \frac{1}{V_u}\left(D_v \frac{C_u - C_l}{L}\right)F \,,\ (wdoC)_l = 0 \quad (20)$$

where:

D_v : the local vertical diffusion coefficients from Pohlmann's model simulation, averaged over the interface

L : the length scale for vertical diffusion

F : the area of the interface

The length scale L was derived from temperature and nutrient observations during the Fladenground Experiment in 1976 (FLEX'76) to be 20 m (Soetje & Huber, 1980).

4.3. TECHNICAL FLOW ADJUSTMENT FOR FIXED BOX VOLUMES

The transport data for 1988 and 1989 from Pohlmann's model provide an annual water balance for the ERSEM boxes of up to about 0.5% (see Table 2). Changed to daily balances, the maximum daily volume change due to surface elevation during 1988 varies between 0.9 and 2.2% of the volumes of the boxes. The difference of the daily water content (between the start and the end of the year) fluctuates by for instance 14.7 km^3 for box 1, which is about 0.9% of the box volume. The mean volume change

due to surface elevation for box 9, with a volume of 602 km^3, corresponds to a volume of 13.82 km^3, which represents 2.2%, and the maximum value of 45.12 km^3 accounts for 7.4% of the box volume. The effects are stronger for the shallow boxes 8 and 9 than for the large boxes 1 to 5.

As a consequence, the ERSEM simulation runs for a conservative tracer such as salt, using daily transport forcing, generate small fluctuations of the salt concentrations when initialized and driven with constant salinity, because in the calculation of the transports by the circulation model the sea surface elevation is taken into account, whereas in the formulation of the ERSEM box model the volumes of the boxes are assumed to be constant.

To use the transports from the circulation model in ERSEM with fixed box volumes, the transports calculated according to the foregoing sections were adjusted to exactly balance zero in each box at each time step. This was done in order to avoid any small deviation from continuity at the very base of the ecosystem and to ensure that any gap in the budgets of chemical and biological state variables was attributable to their specific processes and not caused by missing continuity of water. In setting up the ERSEM ecosystem model, which requires a variety of modules covering several trophical levels to be combined, and hundreds of fluxes interacting between them to be checked, this is a reasonable conclusion.

For this purpose the daily values of transport have been corrected by a linear optimization method to achieve a mass balance equal to zero (Gill *et al.*, 1981). In order to allow the linear optimization method to correct the daily transport data within a realistic level, the high variability of the daily transport time series had to be smoothed first. Therefore a running 30-day averaging was applied, sacrificing short-term variability in horizontal advective flow for the sake of mass balanced transport. The flushing times of the ERSEM boxes (Table 3; see also Lenhart, 1990) show that the time scale appropriate for these boxes is about one month. Although the boxes are flushed at different rates when considering the flushing per unit volume (Radach, 1992), running 30-day averages to the time series of daily horizontal transports are sufficient to represent the flow system. Now it was possible to use the linear interpolation method by allowing the transports to change within the reasonable range of less than 5% in the interior and less than 10% at the boundaries of the North Sea.

The treatment of the transport forcing data as well as the resulting transport is presented in Figs 10a to 10d for 1988 and in Figs 10e to 10h for 1989. Figs 10a and 10e present the integrated time series for the water inflow from box 6 into box 7 for 1988 and 1989, respectively. In section 3.4. it was shown that this inflow, in combination with the flow from box 4 to box 7, plays a major role in how the northern circulation system influences the southern. In Figs 10b and 10f the time series after applying the 30-day running mean is shown together with the time series which is already mass balanced. Only in Fig. 10f can a difference between the two time series be noticed at the beginning of the year. The reduction of the variability is quite obvious, since the strong peaks in the water inflow time series have disappeared. However, the main characteristic between the years can be distinguished, for instance the much stronger inflow at the beginning of 1988.

For the performance of ERSEM as a whole it is important that the modifications of the water transports should not result in distortion of concentrations and fluxes of the chemical and biological state variables. As an example the effects on the state variable phosphate are presented. The actual transport of phosphate through the boundary between boxes 6 and 7 is presented in Figs 10c and 10g, using Eq. 4 for 1988 and 1989, respectively. The corresponding phosphate concentrations for boxes 6 and 7 are shown in Figs 10d and 10h. While the concentration of box 6 is used in Eq. 4 for calculating the phosphate transport presented in Figs 10c and 10d, the phosphate concentration in box 7 is the one resulting from all process contributions described in Eq. 3, of which the phosphate transport presented, in combination with the rest of the boundaries of box 7, is only the part describing horizontal advective transport (whiN1p with N1p representing PO_4). The mass balanced water transport time series for the two years (Figs 10b and 10f) showing a seasonal signal are modulated by the phosphate concentration in the upstream box of the flow, which also has a strong seasonal signal. However, as Figs 10d and 10h show, the horizontal gradient is small between the boxes.

This is important for judging the effect of the transport as well as that of the vertical diffusion on the concentration of, for instance, phosphate within the boxes. In Figs 11a to 11f the process contributions of inflow and outflow as well as of vertical diffusion in and out of the box are presented cumulatively over 1988, exemplified for boxes 2 and 10. In addition, the amount of phosphate is plotted as time series over the year. For box 2 (Fig. 11a) both, the horizontal transport in (wtiN1p) and out (wtoN1p) are much higher than the vertical diffusion into box 2 (wdiN1p). Vertical diffusion out of box 2 (wdoN1p) is zero all the time. However, the difference between advective phosphate in- and outflow is small for box 2 and almost vanishing for box 10 (Fig. 11b). This is the effect of the very small horizontal gradient of phosphate, shown here as one representative nutrient modelled in ERSEM. In box 2 (Fig. 11a) the difference between the inflow and the outflow starts to increase when the concentration of phosphate is reduced at the beginning of the spring bloom. In summer the outflow of phosphate hardly shows any increase, since the concentration determines the phosphate transport strongly. Because box 2 has an external boundary to

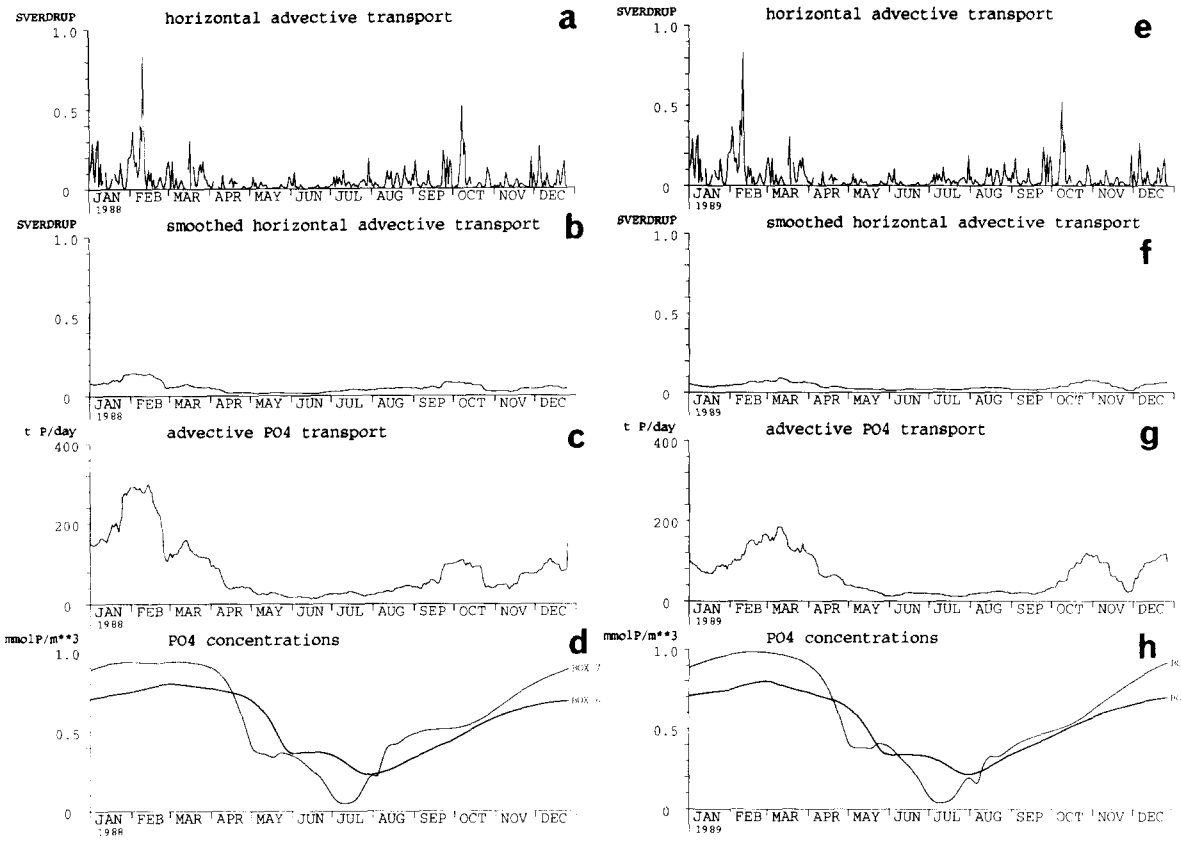

Fig. 10. Effects of smoothed advective water transports on phosphate: Annual time series of daily a. horizontal advective water transport (in Sverdrup), b. smoothed horizontal advective water transport (in Sverdrup), by applying a 30-days averaging, c. advective phosphate transport (in t $P \cdot a^{-1}$) from box 6 to box 7, d. phosphate concentrations (in mmol $P \cdot m^{-3} \cdot d^{-1}$) in boxes 6 (thick line) and 7 (thin line) for 1988, and e. as a, f. as b, g. as c. and h. as d. for 1989, respectively.

the North Atlantic, where higher concentrations are prescribed as boundary values, a higher phosphate transport into the box can be preserved. For box 10, with no external boundaries, this is not the case and therefore cumulative in- and outflow increase little during the nutrient-limited period. One can clearly see the start of the vertical diffusion into box 2 with the beginning of the phosphate limitation in the box. Since box 10 as a coastal box has no thermocline interface there is no vertical diffusion acting in box 10.

Figs 11c and 11d present the cumulative curves for the physical transport of phosphate as well as for the amount of phosphate for a simulation, where the highly variable water transport time series as presented in Figs 10a and 10e are applied. Note that the cumulative curves for in- and outflow of phosphate reach the same level at the end of the year and have exactly the same shape as in Figs 11a and 11b. Moreover, the curves of the resulting amount of phosphate for boxes 2 and 10 show hardly any difference. The only difference observed is the smoother curves from the standard ERSEM simulation in comparison to the results from the simulation forced by the highly variable GCM integrated water flows. But this showed no noticable effect on the rest of the system.

This is readily understandable when looking at the net advective transport and the net vertical diffusive transport cumulated over the year, as shown in Fig. 12, together with the time series of the amount of phosphate for box 2. Fig. 12a presents the standard ERSEM simulation with the mass balanced transport data and Fig. 12b the model results using the highly variable integrated GCM data as forcing for the horizontal advective transport. The simulation results obtained by using net horizontal water flow as forcing are given in Fig. 12c. It is obvious that the resulting cumulative net phosphate transport (TRANS) is in the order of the amount of phosphate itself, whereas the vertical diffusive transport is the dominant physical process. The lack of horizontal gradients of the nutri-

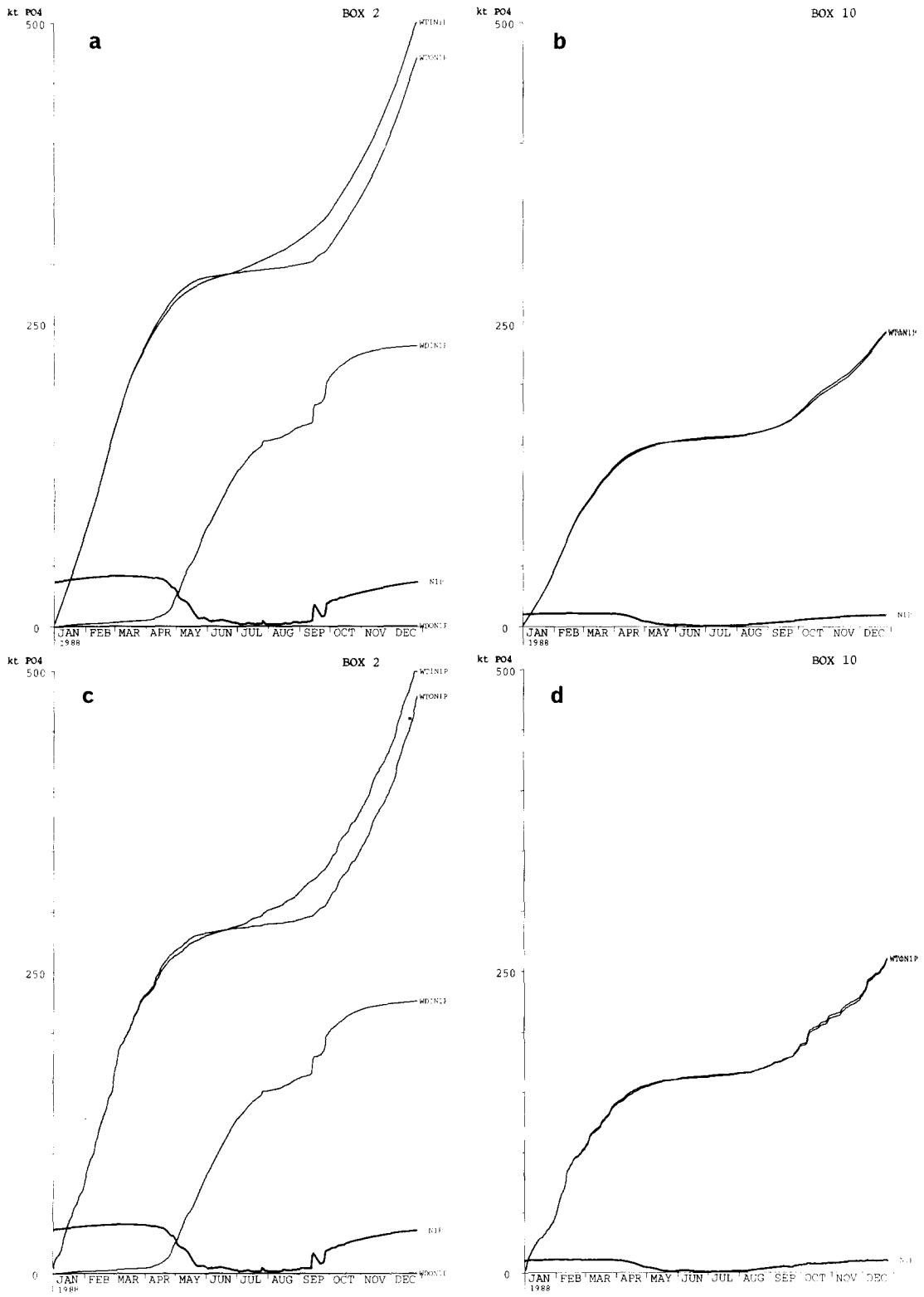
kt PO4
500
250
0
a
BOX 2
WTINIP
WTONIP
WDINIP
N1P
WTONIP
JAN FEB MAR APR MAY JUN JUL AUG SEP OCT NOV DEC
1988
kt PO4
500
250
0
b
BOX 10
WTONIP
N1P
JAN FEB MAR APR MAY JUN JUL AUG SEP OCT NOV DEC
1988
kt PO4
500
250
0
c
BOX 2
WTINIP
WTONIP
WDINIP
N1P
WTONIP
JAN FEB MAR APR MAY JUN JUL AUG SEP OCT NOV DEC
1988
kt PO4
500
250
0
d
BOX 10
WTONIP
JAN FEB MAR APR MAY JUN JUL AUG SEP OCT NOV DEC
1988

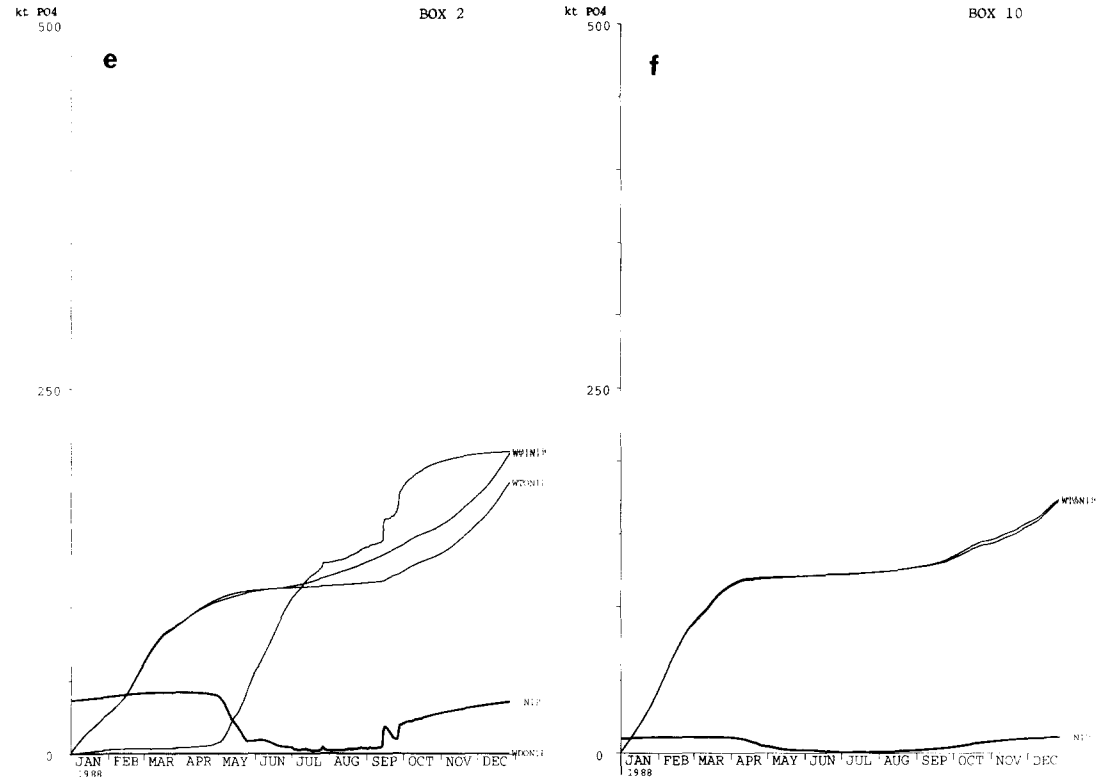

Fig. 11. Effects of smoothed gross and net water transports on the terms of the phosphate budget: Annual cumulative budget for phosphate either simulated by the standard simulation (smoothed gross transports) a. in box 2 and b. in box 10, or simulated by using the original gross transport time series c. in box 2 and d. in box 10, and simulated by using the net smoothed transport time series e. in box 2, and f. in box 10. The gross horizontal advective transports into and out of the box (wtiN1p, wtoN1p) and gross vertical diffusion into and out of (wdiN1p, wdoN1p) are shown together with the phosphate concentration (N1p).

ent phosphate leads to the low impact of horizontal advective transport on the individual phosphate behaviour. Therefore the difference between using a highly variable forcing and a smoothed forcing as used in ERSEM can only be noticed at the boundaries when strongly differing boundary values are applied in contrast to the downstream box concentration.

4.4. INTRINSIC PROBLEMS OF THE COUPLING

The compromise between the need to resolve important scales and the ability to implement a code for ERSEM which allows us to perform annual or even longer simulations on workstations has led to the use of the ERSEM boxes as the smallest spatial scale and a day as the smallest temporal scale. Thus we have to accept approximation errors, the magnitude of which can partly be estimated beforehand and has partly been investigated by systematic numerical experiments with ERSEM.

The resolution of the grid provided by the boxes is of the order of several hundred kilometres. This grid is able to resolve basin-wide structures of the North Sea fields. As a result of the applied advection scheme there is a considerable numerical diffusion at work which, to a first-order estimate, obeys the expression $u \cdot L_B$ (Roache, 1972), where u is the average advection velocity and L_B the average grid scale dimension of the box size. We arrive at a (numerical) diffusion coefficient as large as 10^4 $m^2 \cdot s^{-1}$ if typical values (u = 0.1 $m \cdot s^{-1}$, L_B = 100 km) are assumed. Numerical studies in combination with observations (Maier-Reimer, 1975; Pohlmann *et al.*, 1987) on the dispersion of radioactivity released from Sellafield and La Hague, respectively, arrive at a value of (only) 25 $m^2 \cdot s^{-1}$. Thus, it is justified to neglect horizontal turbulent diffusion as an additional physical process in Eq. 1, because the numerical diffusion coefficient is already larger than the physical one.

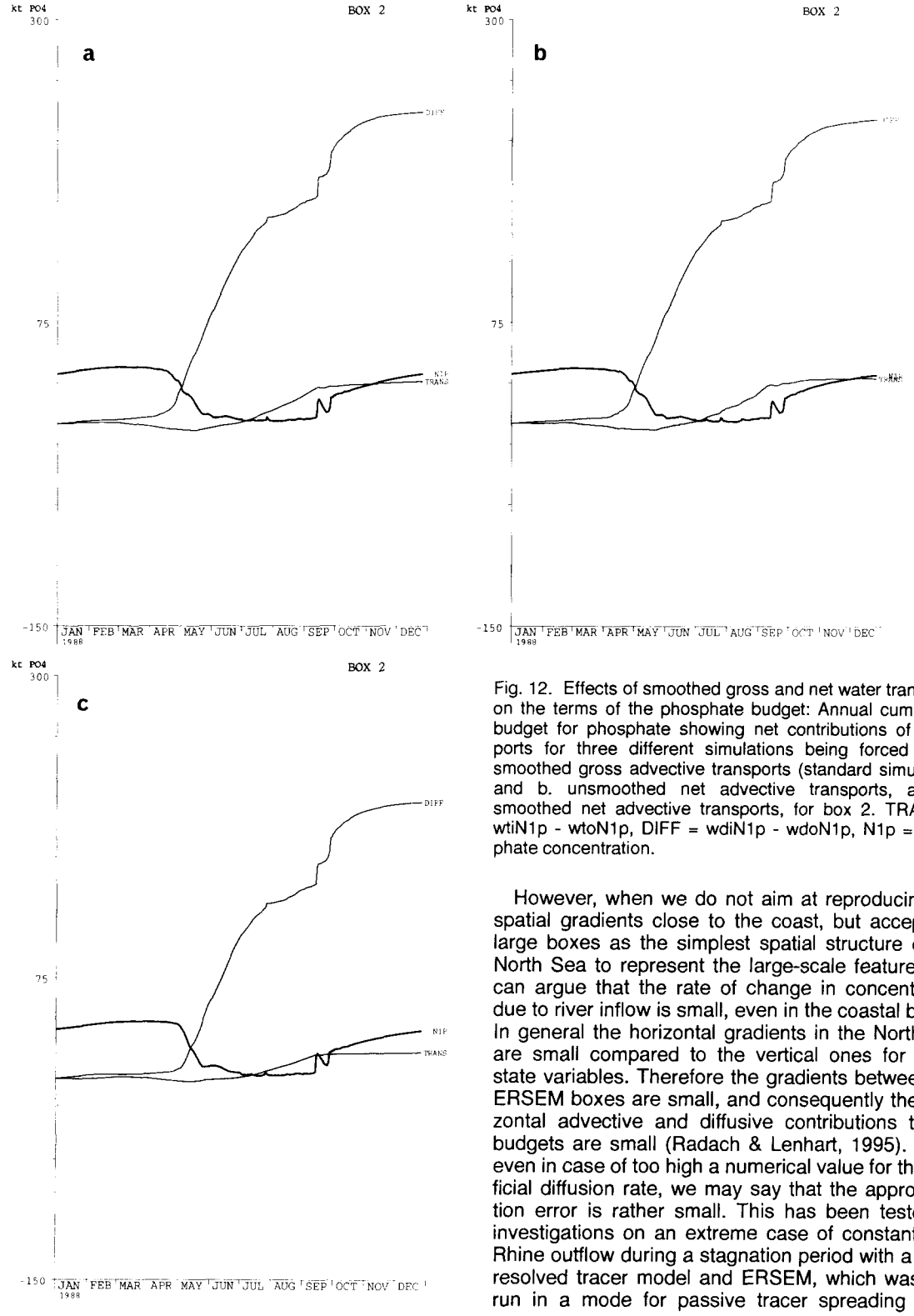

Fig. 12. Effects of smoothed gross and net water transports on the terms of the phosphate budget: Annual cumulative budget for phosphate showing net contributions of transports for three different simulations being forced by a. smoothed gross advective transports (standard simulation) and b. unsmoothed net advective transports, and c. smoothed net advective transports, for box 2. TRANS = wtiN1p - wtoN1p, DIFF = wdiN1p - wdoN1p, N1p = phosphate concentration.

However, when we do not aim at reproducing the spatial gradients close to the coast, but accept the large boxes as the simplest spatial structure of the North Sea to represent the large-scale features, we can argue that the rate of change in concentration due to river inflow is small, even in the coastal boxes. In general the horizontal gradients in the North Sea are small compared to the vertical ones for many state variables. Therefore the gradients between the ERSEM boxes are small, and consequently the horizontal advective and diffusive contributions to the budgets are small (Radach & Lenhart, 1995). Thus, even in case of too high a numerical value for the artificial diffusion rate, we may say that the approximation error is rather small. This has been tested by investigations on an extreme case of constant river Rhine outflow during a stagnation period with a finely resolved tracer model and ERSEM, which was also run in a mode for passive tracer spreading using

transports for 1988. The river load entering the sea was not advected away but only dispersed around the river mouth. Assuming summer conditions of 0.2 mmol $P \cdot m^{-3}$, a maximum error of 33% of the concentration occurred for a limited time in box 8 (where the Rhine enters) and box 9, when comparing the concentrations of the nutrient as a passive tracer which is dispersed in ERSEM against those in a finely resolved transport-dispersion model. For winter conditions of 0.8 mmol $P \cdot m^{-3}$ the error was less than 15% in boxes 8 and 9, and less than 4% in all the other boxes. The total North Sea loses 0.3% of its phosphate contents under 'winter conditions' and 1.3% under 'summer conditions' during a one-year run. As the budgets are dominated by local processes in the productive season (see Fig. 12a), the numerical dispersion is of minor importance when judging the results of ERSEM.

Since these case studies suggested using net transport as an appropriate parameterization to reduce numerical diffusion within these large boxes, a test was carried out to use net water transport also in ERSEM. Therefore at each time step the unidirectional net transport was calculated as the difference between the inflow or outflow. In Figs 11e and 11f the resulting cumulative curves for the individual phosphate transports are plotted and can be compared against the Figs 11a and 11b of the ERSEM standard simulation for boxes 2 and 10, respectively. As one would expect from the setup of the net transport, the phosphate in- and outflow show much lower levels than the standard simulation. But the resulting curve for phosphate shows only a minor change in box 2, with a stronger decline of the phosphate amount in the box during the spring bloom in May, and no obvious difference for box 10. A comparison of net horizontal phosphate transport, *i.e.*, the difference between advective in- and outflow of phosphate cumulative over 1988 (Fig. 12c), with the results from the standard simulation (Fig. 12a) shows minor changes between the transports in box 2. The phosphate concentration of the standard simulation is slightly higher towards the end of the simulation, but again it is noticeable that the vertical diffusion is the major physical process acting on the phosphate concentration.

4.5. THE IMPACT OF VERTICAL DIFFUSION ON ERSEM DYNAMICS

The vertical diffusion acting on the 30-m thermocline layer introduces a strong physical signal within the pelagic biota. Even though the vertical diffusion is much weaker than the advective transport in terms of transported mass, the strong vertical gradients of, for instance, nutrients have a pronounced effect on the biochemical environment. In Fig. 13 the effects of the vertical diffusion can be followed up to the trophic level of phytoplankton. Fig. 13a shows the time series of the vertical diffusion coefficients for the Norwegian Trench box 3 for 1989. These vertical diffusion coefficients were calculated at the 30-m thermocline layer separating an upper (from 0 - 30 m depth) and a lower (from 30 m depth to the bottom) box. The time series shows a typical seasonal characteristic with low values during the summer period, lasting from April until the end of September. The diffusive flux of a nutrient such as phosphate is determined by the gradient between the upper and lower boxes (see section 4.2.4.). The fluxes of phosphate by vertical diffusion into and out of the upper box are presented in Figs 13b and 13c. The corresponding phosphate concentrations for both boxes are shown in Fig. 13d. The lower box remains at a high nutrient concentration throughout the year whereas within the upper box the concentration decreases from April until September due to nutrient uptake by algae. Even though there are high vertical diffusion coefficients at the beginning and the end of the year, the corresponding phosphate flux into the upper box is very low. Only when a gradient is developing between the two layers are there some flux events into the upper box. These events fade away quickly because the vertical diffusion coefficient drops to zero during the summer. Wind events towards the autumn result in high values for the vertical diffusion coefficient again. In combination with a strong nutrient gradient between the two layers, because of algal uptake in the upper euphotic layer, strong fluxes occur of phosphate into the upper layer which lead to a rise of the concentration in the upper box.

One extremely strong event can be observed at the beginning of August, which can be followed in the concentration of phosphate as a peak within the low summer surface concentration. The result of this peak in the nutrient concentration within the euphotic upper layer can even be seen as an increase in the total phytoplankton biomass. There are a number of such coincidences between nutrient fluxes and at least observable rises in the nutrient concentration within the upper layer. The event in August is just one major event after the summer stagnation which demonstrates the effect of the nutrient gradient between the boxes when the actual value for the vertical diffusion coefficient is still very low.

Finally the vertical diffusive flux of phosphate into the upper box leads to a balance between the boxes indicated by the winter concentration. Then, as at the beginning of the year, also small fluxes out of the upper box into the lower box can occur in order to balance the box concentrations in both layers.

This example shows very clearly the importance of the strong vertical gradients in combination with a relatively weak physical forcing in contrast to effects of horizontal advection. In the absence of strong horizontal gradients which cannot be resolved by the present box structure, the local dynamics in the vertical dominate over large-scale horizontal transport

processes.

5. DISCUSSION AND CONCLUSIONS

The ERSEM ecosystem model takes into account the gross features of the North Sea physical system by using a box setup of modified ICES boxes. Their modifications, namely the vertical separation of the deep boxes in the central and northern North Sea, added a considerable amount of realism by representing of the biologically important upper mixed layer.

By mapping the finely-resolved flow fields from an advanced existing general circulation model for the North Sea on the ERSEM boxes indicated, the gross features of the North Sea circulation as well as the individual characteristics of the ERSEM boxes, for instance their flushing times, could be maintained. The water budgets for the ERSEM boxes are shown to be annually well balanced with a remaining net difference between in- and outflow of less than 0.5% of the corresponding inflow value. Due to the restriction of the fixed box volumes, the effects of the daily varying sea surface elevation could not be taken into account explicitly without changing the ERSEM formulation as a whole. Since a mass balance equal to zero had to be achieved for reasons of model transparency (see section 4.3.), the daily transport values were corrected by linear optimization after smoothing the transport time series by a 30-day running average filtering out a great deal of short-term variability from the time series of water transports. Since the horizontal gradients (such as for the nutrient concentrations) are small, the resulting nutrient transports are only marginally affected. Nevertheless major differences between different years can clearly be observed.

Within the structural setup the dominant role of vertical diffusion as the major physical forcing during the nutrient-limited part of the year has clearly been shown. Here the strong vertical gradient allows for intensive nutrient fluxes into the upper boxes by relatively weak physical forcing. The effect of these fluxes can be followed not only within the nutrient state variable itself but also in the biota, for instance in the response of the phytoplankton to the change in nutrient concentration.

In order to test the parameterization for the implemention of the transport derived from the GCM model, comparisons of model results from ERSEM against a finely resolved tracer model were carried out, in which freshwater was used as a tracer, introducing strong horizontal gradients when spreading from point sources. Mapping the results of the finely resolved tracer model onto the ERSEM boxes leads to the conclusion that the net transport should be used as the appropriate parameterization for the transport.

Within the large ERSEM boxes there is considerable numerical diffusion. Therefore the use of the gross transport or of the net transport plus horizontal diffusion leads to an overestimation of horizontal diffusion in the model in comparison to the results from the finely resolved tracer simulation study. However, since the gross box structure of the ERSEM model was not meant to represent strong horizontal gradients and since strong horizontal gradients of nutrient concentration do not occur, as mentioned above, it is not surprising that the implementation of net transports showed only marginal differences in the resulting phosphate concentrations or even in the cumulative curve of the net transport over one year, when compared to the simulation using gross water horizontal transports. Based on the findings from the tracer model study, the net transport will be introduced into the ERSEM standard model as the optimal transport representation in the future. The present use of the gross transports leads to only marginally deviating model results for nutrients.

However, there might be a small effect in the boundary regions where stronger horizontal gradients

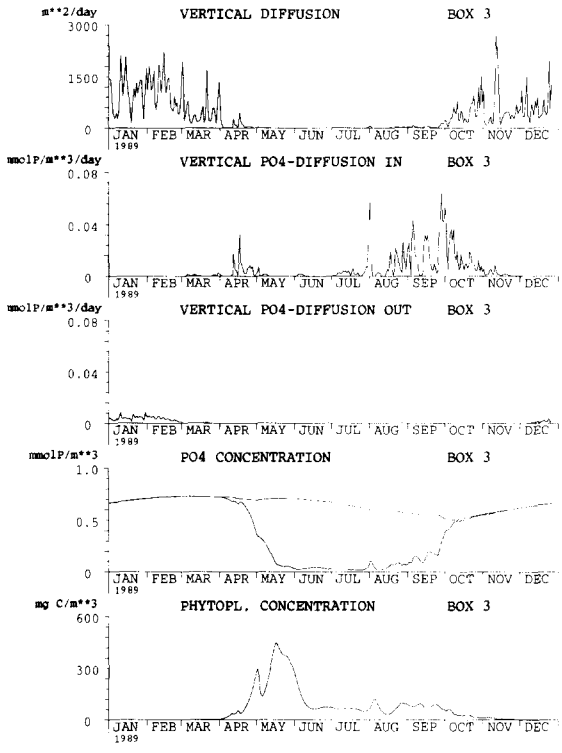

Fig. 13. Influence of vertical diffusion on the ecosystem: a. vertical diffusion rates (in $m^2 \cdot d^{-1}$), b. vertical diffusive influx into box 3, c. vertical diffusive outflux out of box 3, d. concentrations of phosphate in the upper (with summer depletion) and lower layer (without summer depletion) and e. phytoplankton concentration (diatoms plus flagellates) of box 3. Note the effect of the diffusive event in early August in all curves.

can occur or, for instance, in case of regionally different onsets of phytoplankton spring blooms. Regional differences might be smeared out to some degree at times of strong local changes in the concentration. Since these are related to relatively short time intervals, horizontal numerical diffusion will only have a small effect on the yearly cycle.

When considering the aims of the ERSEM model taking into account the ease with which model results can be compared with the aggregated data in the ICES boxes, one can conclude that the gross features of the North Sea are represented well by the given box structure and by the physical forcing applied. In addition, the computational overhead of such a complex model as well as the feasibility of checking hundreds of fluxes between the different submodules made it advisable to start with reproducing only the gross features of the North Sea. Focussing on regions with stronger horizontal gradients such as the coastal regions smaller boxes are needed which are capable of representing these strong gradients. Additional comparisons with tracer studies have to be carried out with the aim to find a box structure which will allow us to use the full potential of the stored GCM simulation data when applying net advective transports in combination with horizontal diffusive transports.

By mapping the flow induced high-frequency variability onto the ERSEM boxes, this variability was already reduced. The chemical and biological variables thus exhibit considerable less variability than the original forcing itself, although the ecosystem dynamics are different in the simulations for 1988 and 1989 (Radach & Lenhart, 1995). From the purely physical simulations as well as from previous phytoplankton simulations in the North Sea, independent of the formulation as 1-D (Ridderinkhof, 1992; Radach & Moll, 1993) or 3-D model (Pohlmann, 1991), we know that the highly variable marine system 'North Sea' can be simulated only to a satisfactory degree of realism if the temporal small-scale meteorological forcing is imposed on the system (or if an adequate parameterization is applied).

Although the 1-D plankton simulations suggest that the high-frequency meteorological variability is buffered during the year, and the annual plankton production yield is very similar between the years (Radach & Moll, 1993), we have to note that the often used mean or smoothed fields will activate only part of the reaction potential of the system.

From these findings two important conclusions can be drawn for the hydrodynamic forcing introduced into the ERSEM simulations. Firstly, the forcing for ERSEM must be introduced on a time scale of a day or less to express the hydrodynamical variability. This approach has a greater potential to simulate ecosystem dynamics which are comparable to observations. Secondly, to enable higher variability to be transferred from the physical forcing to the temporal development of the chemical and biological state variables a finer spatial resolution seems to be necessary.

One arbitrarily chosen year of forcing will give only one realization out of an infinity of possibilities and for such a specific year only a very limited number of observations will be available. In general, the necessary initial and boundary conditions are not available to reproduce an observed realization by a model simulation. In our view a model such as ERSEM should be validated by comparing its potential dynamics with the observed variability rather than with only one observed case. This means that all data from comparable dynamical situations, *i.e.* from several annual cycles, have to be combined to judge the validity of the model results.

It remains a future task to investigate how much of physical variability has been buffered by the biological system described in ERSEM and how much of the biological variability is due to the implementation scheme for the hydrodynamic forcing and its numerical realization. The conclusion from the fact that a great deal of physical variability disappears is then, firstly, that the appropriate box size and time step should be investigated by numerical experiments, to ensure both the realization of the effect of the small-scale physical forcing and the least numerical approximation error obtainable under the technical constraints regarding hardware and software. Secondly, it should be investigated under which variable physical forcing the ecosystem model will produce high variable ecosystem state variable evolutions.

Acknowledgements.—This research was funded by the European Union under MAST contract number CT90-0021. We would like to thank our colleagues M. Regener and J. Pätsch for valuable comments on previous versions of the manuscript. Thanks are also due to B. Hellmann for his technical support. We also thank our reviewers and J.G. Baretta-Bekker for their suggestions to improve the paper.

6. REFERENCES

Backhaus, J.O., 1983. A semi-implicit scheme for the shallow water equation for application to shelf sea modelling.—Cont. Shelf Res. **2:** 243-354.

——, 1984. Estimates of the variability of low frequency currents and flushing times of the North Sea. ICES Hydrography Committee, C.M. 1984/C: 24: 1-18.

——, 1985. A three-dimensional model for the simulation of shelf sea dynamics.—Dt. hydrogr. Z. **38:** 167-262.

——, 1989. The North Sea and the climate.—Dana **8:** 69-82.

——, 1990. On the atmospherically induced variability of the circulation of the northwest European shelf sea and related phenomena — a model experiment. In: A.M. Davies. Modelling marine systems. CRC Press, Boca Raton, Florida: Vol. 1: 93-134.

Backhaus, J.O., T. Pohlmann & D. Hainbucher, 1986. Regional aspects of the circulation on the north European shelf. ICES C.M. 1986/C:38: 1-17.

Backhaus, J.O., J. Bartsch, P. Damm, T. Pohlmann & C. Schrumm, 1991. The marine weather bulletin North Sea. ICES Hydrography Committee, C.M. 1991/ C:16:1-17.

Baretta, J.W. & P. Ruardij, 1988. Tidal flat estuaries. Simulation and analysis of the Ems estuary. Ecol. Studies 71. Springer-Verlag, Heidelberg: 1-353.

Baretta, J.W., W. Ebenhöh & P. Ruardij, 1995. The European Regional Seas Ecosystem Model, a complex marine ecosystem model.—Neth. J. Sea Res. **33:** 233-246.

Becker, G., 1981. Beiträge zur Hydrographie und Wärmebilanz der Nordsee.—Dt. hydrogr. Z. **34:** 167-262.

——, 1990. Die Nordsee als physikalisches System. In: J.L. Lozan, W. Lenz, E. Rachor, B. Watermann & H. Von Westernhagen. Warnsignale aus der Nordsee. Parey Verlag, Berlin: 11-27.

Colebrook, J.M., 1979. Continuous plankton records: Seasonal cycles of phytoplankton and copepods in the North Atlantic Ocean and the North Sea.—Mar. Biol. **51:** 23-32.

Dickson, R.R., J.M. Colebrook & E. Svendsen, 1992a. Recent changes in the summer plankton on the North Sea. In: R.R. Dickson, P. Mälkki, G. Radach, R. Saetre & M.P. Sissenwine. Hydrobiological variability in the ICES area, 1980-1989. Mariehamn: 232-242.

Dickson, R.R., P. Mälkki, G. Radach, R. Saetre & M.P. Sissenwine 1992b. Hydrobiological variability in the ICES area, 1980-1989. Hydrobiological variability in the ICES area, 1980-1989, Mariehamn: 1-516.

Fransz, H.G., J.P. Mommaerts & G. Radach, 1991. Ecological modelling of the North Sea.—Neth. J. Sea Res. **28:** 67-140.

Gill, P.E., W. Murray & M.H. Wright, 1981. Practical optimization. Academic Press, London: 1-213.

Goedecke, E., J. Smed & G. Tomczak, 1967. Monatskarten des Salzgehalts der Nordsee.—Dt. hydrogr. Z., Ergänzungsheft B **8:** 1-182.

Hainbucher, D., J.O. Backhaus & T. Pohlmann, 1986. Atlas of climatological and actual seasonal patterns in the North Sea and adjacent shelf regions: 1969-1981. Technical Report 1-86, Institut für Meereskunde, Univ. Hamburg: 1-201.

——, 1987. Transport of conservative passive tracers in the North Sea: first results of a circulation and transport model.—Cont. Shelf Res. **7:** 1161-1179.

ICES, 1962. Mean monthly temperature and salinity of the surface layer of the North Sea and adjacent waters. ICES, Charlottenlund: 1-159.

——, 1983. Study Group on the Flushing times of the North Sea. Coop. Res. Rep. 123, Intern. Council Explor. Sea, Copenhagen: 1-159.

Jakobsen, T.S., 1986. Water exchange through the Danish Straits. In: HELCOM,1986. Water balance of the Baltic Sea. Baltic Sea Environm. Proc. **16:** 81-100.

Kautsky, H., 1985. Distribution and content of different artificial radio nuclides in the water of the North Sea during the years 1977 to 1981.—Dt. hydrogr. Z. **38:** 193-224.

Keeling, C.D. & B. Bolin, 1967. The simultaneous use of chemical tracers in oceanographic studies. I. General theory of reservoir models.—Tellus **19:** 566-581.

Lenhart, H.J., 1990. Phosphatbilanz der Nordsee - eine Abschätzung auf der Grundlage der ICES-Boxen. Diplomarbeit, Fachbereich Geowissenschaften, Univ. Hamburg: 1-111.

Luthardt, H., 1987. Analyse der wassernahen Druck- und Windfelder ber der Nordsee aus Routinebeobachtungen.—Hamburger Geophysikalische Einzelschriften A, **83:** 1-115.

Maier-Reimer, E., 1975. Zum Einfluss eines mittleren Windschubes auf die Restströme der Nordsee.—Dt. hydrogr. Z. **28:** 253-262.

North Sea Task Force, 1993. North Sea Quality Status Report. Oslo and Paris Commission, London: 1-132.

Otto, L., J.T.F. Zimmerman, G.K. Furnes, M. Mork, R. Saetre & G. Becker, 1990. Review of the physical oceanography of the North Sea.—Neth. J. Sea Res. **26:** 161-238.

Pohlmann, T., 1991. Untersuchung hydro- und thermodynamischer Prozesse in der Nordsee mit einem dreidimensionalen numerischen Modell. Dissertation Univ. Hamburg: 1-116.

——, 1995a. Predicting the thermocline in a circulation model of the North Sea. Part I: Model description, calibration, and verification.—Cont. Shelf Res. (in print).

——, 1995b. Calculating the annual cycle of the vertical eddy viscosity in the North Sea with a three dimensional baroclinic shelf sea circulation model.—Cont. Shelf Res. (in print).

Pohlmann, T., J.O. Backhaus & D. Hainbucher, 1987. Validation of a three dimensional dispersion model for CS137 in the north European shelf sea. ICES C.M. 1987/C:34.

Radach, G., 1992. Ecosystem functioning in the German Bight under continental nutrient inputs by rivers.—Estuaries **15:** 477-496.

——, 1994. The general transport equation for an ecosystem box model, driven by simulated 3 D circulation. Techn. Rep. 2-94, Institut für Meereskunde, Univ. Hamburg: 1-20.

Radach, G. & H.J. Lenhart, 1995. Nutrient dynamics in the North Sea: fluxes and budgets in the water column derived from ERSEM.—Neth. J. Sea Res. **33:** 301-335.

Radach, G. & A. Moll, 1990. The importance of stratification for the development of phytoplankton blooms - a simulation study. In: W. Michaelis. Estuarine water quality management. Monitoring, modelling, research. Lecture notes on coastal and estuarine studies. Springer Verlag, Berlin: 389-394.

——, 1993. Estimation of the variability of production by simulating annual cycles of phytoplankton in the central North Sea.—Prog. Oceanogr. **31:** 339-419.

Radach, G., J. Berg & E. Hagmeier, 1986. Annual cycles and phenomena on other time scales in temperature, salinity, nutrients and phytoplankton at Helgoland Reede, 1962 - 1984. ICES C.M. 1986/ C:2: 1-9.

——, 1990. Long-term changes of the annual cycles of meteorological, hydrographic, nutrient and phytoplankton time series at Helgoland and at LV ELBE 1 in the German Bight.—Cont. Shelf Res. **10:** 305-328.

Ridderinkhof, H., 1992. On the effects of variability in meteorological forcing on the vertical structure of a stratified water column.—Cont. Shelf Res. **12:** 25-36.

Roache, P., 1972. Computational fluid dynamics. Hermosa Publishers, Albuquerque, New Mexico: 1-446.

Soetje, K.C. & K. Huber, 1980. A compilation of data on the thermal stratification at the central station in the northern North Sea during FLEX'76.—'Meteor' Forsch.-Ergebn. **A (22):** 69-77.

Stronach, J.A., J.O. Backhaus & T.S. Murty, 1993. An

update on the numerical simulation of oceanographic processes in the waters between Vancouver Island and the mainland: the GF8 model.—Oceanogr. mar. biol. ann. Rev. **31:** 1-86.

Tomczak, G. & E. Goedecke, 1962. Monatskarten der Temperatur der Nordsee dargestellt für verschiedene Tiefenhorizonte. —Dt. hydrogr. Z. **7:** 1-112.

Uncles, R.J., 1988. Coupling of hydrodynamic and ecosystem modelling applied to tidal estuaries. In: B.O. Jansson. Lecture notes on coastal and estuarine studies 22: Coastal-offshore interactions. Springer-Verlag, Berlin: 309-354.